SCHOOL OF MECHANICAL,
INDUSTRIAL & AERONAUTICAL
ENGINEERING

MECHATRONICS II: MECN4029A - PROJECT ASSIGNMENT

MECHATRONIC SYSTEMS DESIGN: ANALYSIS AND CONTROL

PROJECT B: SOLAR TRACKER

Group: 15

Members:

848906 - T. Ndwandwe

2083932 - T. Mavhungu

2116478 – B. Vilakazi

1913357 – F. Torres

An MECN4029A - Mechatronics II group assignment submitted to the Faculty of Engineering and the Built Environment, University of the Witwatersrand, Johannesburg, in partial fulfilment of the requirements for the degree of Bachelor of Science in Engineering.

Johannesburg, May 2024

EXECUTIVE SUMMARY

The project entailed the design and simulation of a single-axis solar tracker system. The system was modelled as an armature-controlled DC motor with an inertial load. The uncontrolled system was found to be marginally stable, necessitating the implementation of a controller. Various PID controller schemes were tested, and the PID controller was selected due to its superior performance in minimizing both transient and steady-state errors. The PID controller effectively met the desired performance specifications, ensuring precise tracking of the sun's position and maximizing energy capture. The system's response was evaluated using solar position data for summer and winter months, demonstrating its effectiveness in different environmental conditions. The implementation of the PID controller significantly enhanced the solar tracker's performance, making it a viable solution for improving energy generation efficiency in solar the Kalkbut Solar farm.

Table of Contents

LIST OF FIGURES

LIST OF TABLES

NOMENCLATURE

Symbol	Units	Description
e_a	V	Armature voltage
V_R	V	Voltage of resistor
V_L	V	Voltage across inductor
e_m	V	Motor voltage
i_a	A	Armature current
R	Ω	Resistance
L_a	H	Inductance
k_m	$V/rad/s$	Back EMF Constant
θ_m	rad	Motor angle
θ_s	rad	Shaft angle
n	-	Gear ratio
$J_{P,eq}$	m^4	Equivalent panel polar moment of inertia
J_P	m^4	Panel polar moment of inertia
m_P	kg	Panel mass
l	m	length
r	m	Shaft radius
θ_P	rad	Panel angle
$\dot{\theta}_P$	rad/s	Angular velocity
$\ddot{\theta}_P$	rad/s^2	Angular acceleration
g	m/s^2	Gravitational acceleration
ρ	kg/m^3	Air density
A	m^2	Frontal area of solar panel
v	m/s	Wind velocity
C_D	-	Drag coefficient
C_L	-	Lift coefficient
T_S	Nm	Shaft torque
T_P	Nm	Panel torque
c	-	Damping coefficient
J_S	m^4	Shaft polar moment of inertia
T_m	Nm	Motor torque
k_t	Nm/A	Motor Torque Constant

1. INTRODUCTION

The Kalkbut farmhouse, which is South Africa’s first solar farm, with its current capacity of 75 MW, plays a significant role in contributing to South Africa's renewable energy goals [1]. While the current fixed-tilt system undoubtedly generates clean energy, implementing solar tracking technology has the potential to significantly increase the facility's output. Solar trackers are generally more expensive than fixed-tilt systems. However, for large-scale solar facilities like the Karoo Renewable Energy Facility, the increased energy production can lead to significant economic benefits over time.

Figure 1: The Solar Arrays at the Kalkbut Farmhouse [1]

Solar trackers are devices that move solar panels throughout the day to follow the sun's path in the sky. This increases the amount of sunlight hitting the panels, which can generate 25-45% more electricity compared to fixed-tilt systems [2]. There are two main types of solar trackers, single-axis trackers, and dual-axis trackers. Single axis trackers follow the sun east to west, tilting the panels throughout the day for optimal sun exposure whereas dual-axis trackers can adjust both east-west and north-south, maximizing sunlight capture throughout the year.

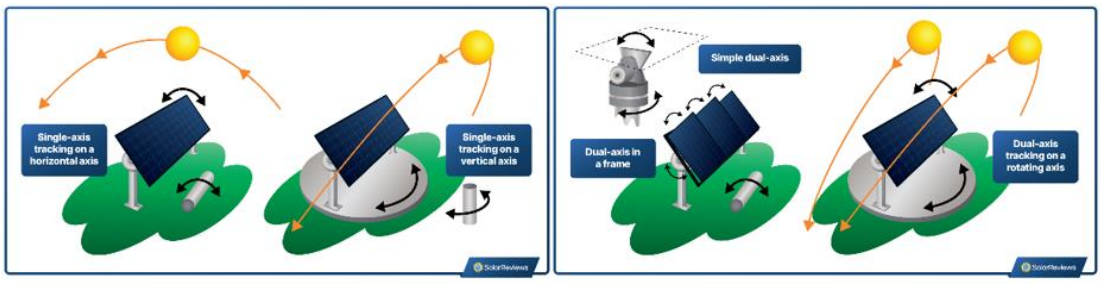

Figure 2:Single and dual axis solar tracking configurations [2]

This project aims to design and simulate a control system for a single-axis solar tracker system to be implemented at the Kalkbut farmhouse solar farm, resulting in a significant increase in energy generation compared to the existing fixed-tilt system at the solar farm.

2. PERFORMANCE SPECIFICATIONS

The desired tracking accuracy for the solar tracker is ± 0.5°. Below are the performance specifications for the solar tracker.

2.1. Time Domain Performance Specifications

- Max overshoot: < (1.2 of y_{ss}) 20%
- Peak time < 2 seconds
- Rise time: < 1.8 seconds
- Settling time: 2-5% of y_{ss} < 4 seconds
- Delay time: time taken for step response to reach 50% of y_{ss} < 2 seconds.
- Decay ratio: 2^{nd} peak/1^{st} peak < 0.3.
- Steady state error: as close to 0

2.2. Frequency Domain Performance Specifications

- Amplitude ratio = 1
- Phase angle = 0
- Peak amplitude ratio between 1.1 and 1.5

3. System Modelling

3.1. Physical Modelling

Solar farms are essentially giant collections of solar arrays. An array itself is a group of solar panels wired together to capture sunlight and produce electricity. These panels are arranged in rows on metal frames, angled to face the sun for maximum efficiency. Many solar farms use single axis tracking systems, which means the panels can rotate throughout the day to follow the sun's movement across the sky. The electricity produced by the solar arrays is converted from direct current (DC) to alternating current (AC) by inverters, so it can be fed into the power grid.

The solar array sits on a single axis tracking mechanism, which allows it to tilt along one axis follow the sun's path throughout the day. A DC gear motor sized for the panel weight, wind load, and desired tracking speed provides the driving force. A potentiometer mounted on the tracking mechanism's axis acts as a real-time position sensor, converting the tilt angle into a voltage signal for the control system. Table 1 lists out the specifications for the solar array.

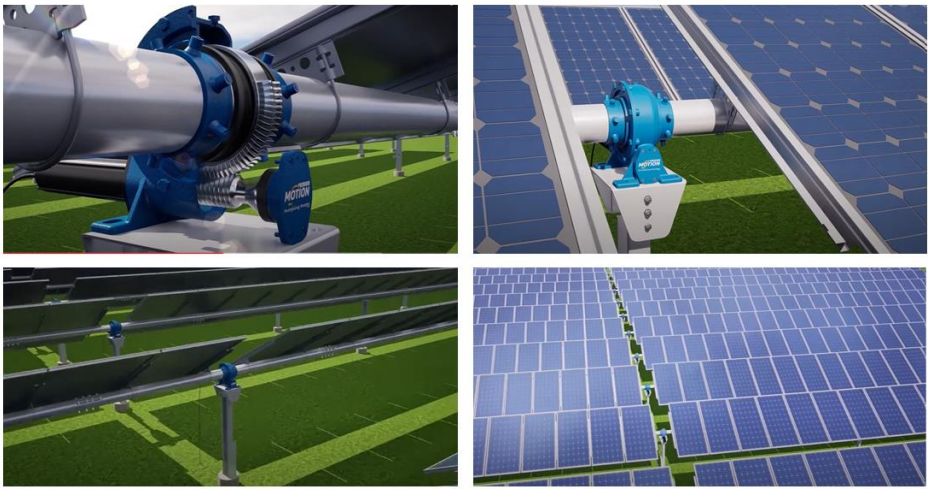

Figure 3: CAD rendering for proposed solar tracking system [3]

To optimize our single-axis solar tracker design, we'll prioritize a time-based tracking strategy for its simplicity and cost-effectiveness. We'll select a DC motor with sufficient torque and a gear reduction system for precise panel movement. The tracker's structure will use high-strength, lightweight materials to handle panel weight, wind loads, and potential snow based on the installation location. We'll decide between LDRs or explore advanced sun trackers for the control system's sensors, considering the trade-off between cost and efficiency. Throughout the design process, we'll prioritize a balance between affordability, reasonable efficiency gains, and durability. The system will automatically secure the panels during high winds and its tracking will be programmed based on the site's location and season. We'll also consider maintenance access and potentially a solar-powered or low-power design for the control system.

Table 1: Solar Array Specifications

Array Row Dimensions (total footprint) [mm]	1400x2000x8500
Array Mass [kg]	1845
Array Inertia [$Kg \cdot m^2$]	399.14
Array Power (Peak) [kWp]	75
No of Array Panels	75
1 Panel Dimensions [mm]	1765x1048x35
1 Panel mass [kg]	20.5
1 Panel Power Rating (Peak) [W]	380
Drive Shaft Dimensions (Length, OD, Thk) [mm]	7200x140x10 (x11 shafts)
Mounting distance $(l + r_{drive\ shaft})$ [mm]	(50+70) =120
Driveshaft Mass (total) [kg]	2540
Driveshaft Inertia [$Kg \cdot m^2$]	12.45
Motor	24VDC
Motor Damping Constant [$N \cdot m/(\frac{rad}{s})$]	$8.1449x10^{-6}$
Motor MOI [$kg \cdot mm^2$]	1.8
Slew Drive (Nominal Sizes OD x ID x Thk) [mm]	350 x 145 x 108
Motor Torque Constant [N-m/A]	0.062
Back EMF Constant [V/rad/s]	0.062
Winding Resistance @ Ambient [Ohm]	1
Shaft Material	4130 Alloy Steel Tubing
Upington Air Density @ 20ºC (293°K) [kg/m³]	1.09
Gear Ratio	62:1
C_D	0.29
C_L	0.25

3.2. Mathematical Modelling

With reference to the physical model, the mathematical model can be derived from the underlying physics principles.

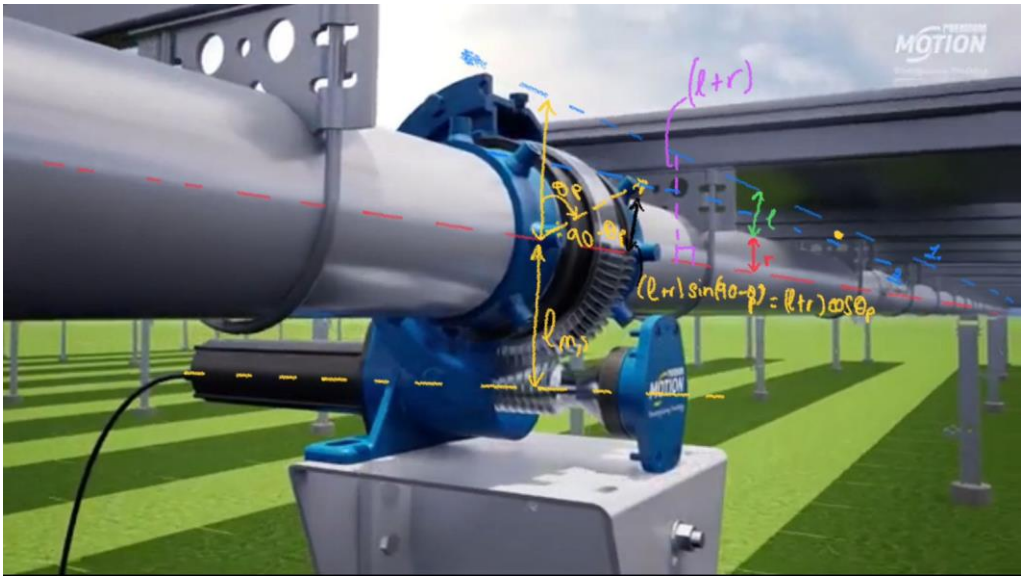

Figure 4: Annotated solar panel system [3]

- Design decision.

The system was modelled as an armature-controlled DC motor with an inertial load. This solar panel system is an electromechanical system where the motor is used to rotate the shaft. An armature-controlled DC motor model was chosen over a field-controlled DC-motor model since we need direct control over the motors voltage to allow the desired shaft angle to be achieved [4].

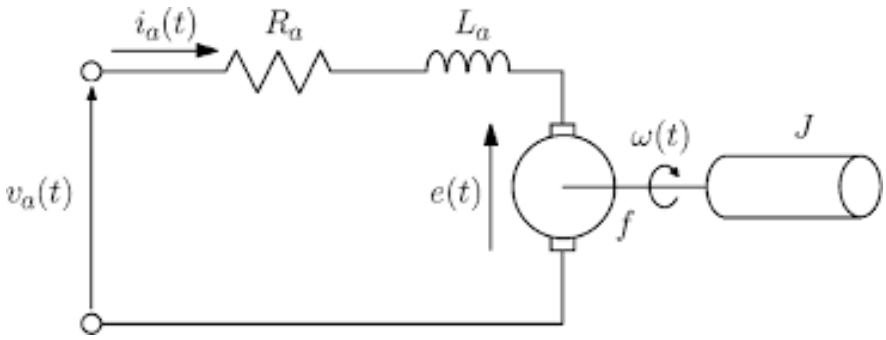

Figure 5: Armature Controlled DC Motor with an inertial load [4].

- Assumptions

- No inductance in circuit.
- No vortex shedding.
- Small angle approximations are valid.
- $k_t \; and \; k_m$ are constant.

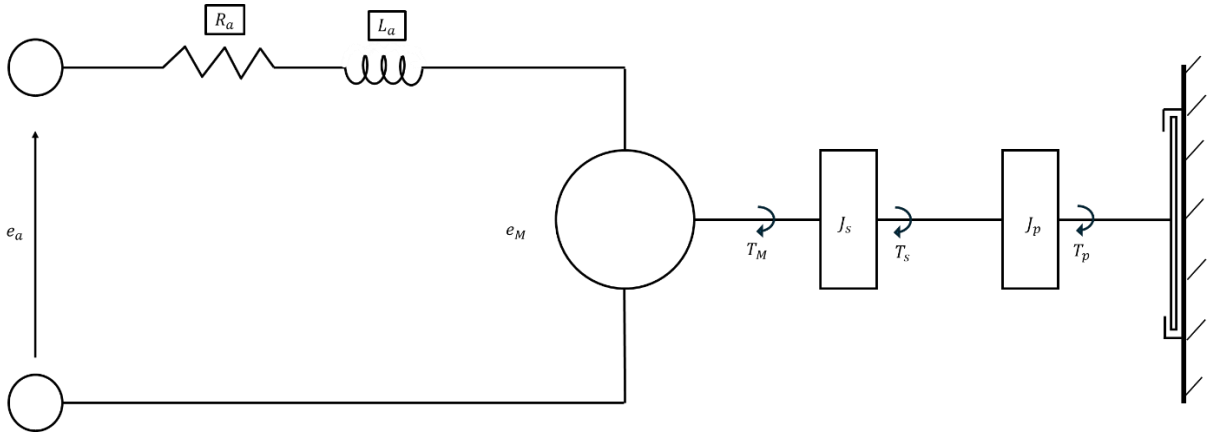

Figure 6: System Diagram

Using Kirchhoff's voltage law:

$$e_a = V_R + V_L + e_m \tag{1}$$

$$e_a = i_a R + L_a \frac{di_a}{dt} + k_m \dot{\theta}_m \tag{2}$$

Assuming no inductance and accounting for gear ratio $\theta_m = n\theta_s$

$$e_a = i_a R + k_m n \dot{\theta}_s \tag{3}$$

$$i_a = \frac{1}{R}\left(e_a - k_m n \dot{\theta}_s\right) \tag{4}$$

- Panel

Polar moment of inertia for the rotating solar panel

$$J_{P,eq} = J_P + m_P l^2 \tag{5}$$

$$J_{P,eq} = J_P + m_P\left((l + r)(\cos 90 - \theta_P)\right)^2 \tag{6}$$

$$J_{P,eq} = J_P + \frac{1}{2} m_P (l + r)^2 \sin^2 \theta_P \tag{7}$$

$$J_{P,eq} = J_P + \frac{1}{2} m_P (l + r)^2 (1 - \cos 2\theta_P) \tag{8}$$

Using newtons second law for rotation.

$$\sum M_o = J_{P,eq}\ddot{\theta}_P \tag{9}$$

$$-(m_P g \sin\theta_P)(l+r) + \left(\frac{1}{2}\rho A v^2\right)(l+r)(C_D \cos\theta_P + C_L \cos\theta_P) = \left[J_P + \frac{1}{2}m_P(l+r)^2(1-\cos 2\theta_P)\right]\ddot{\theta}_P \tag{10}$$

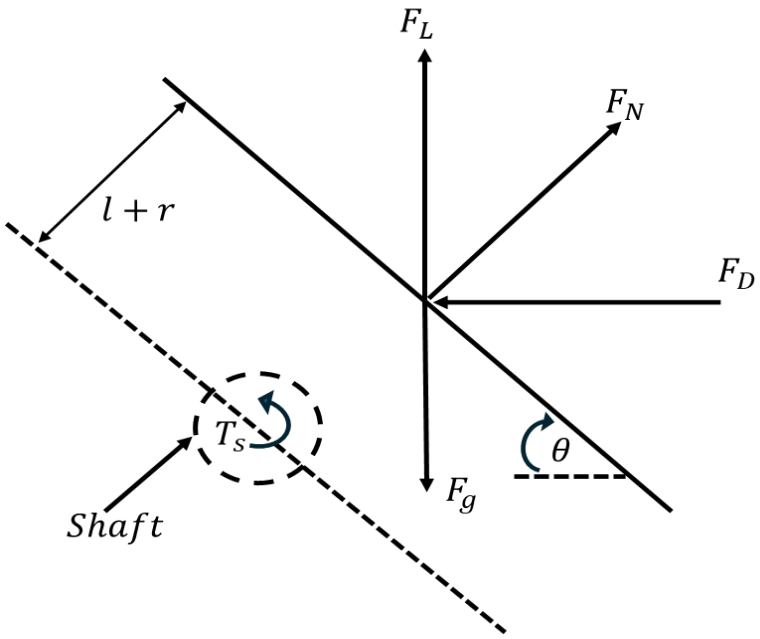

Figure 7: Panel Free-Body Diagram

- Combined Load

$$+\circlearrowleft \sum M_o = (J_S + J_{P,eq})\ddot{\theta}_P \tag{11}$$

$$T_S + T_P - c\dot{\theta}_P = (J_S + J_{P,eq})\ddot{\theta}_P \tag{12}$$

where $T_S = nT_m = nk_t i_a$, and $T_P = (10)$,

$$\begin{aligned} nk_t i_a - m_P g \sin\theta_P\,(l+r) + \frac{1}{2}\rho A v^2 (l+r)(C_D\cos\theta_P + C_L \sin\theta_P) - c\dot{\theta}_P \\ = \left(J_S + J_P + \frac{1}{2}m_P(l+r)^2(1-\cos 2\theta_P)\right)\ddot{\theta}_P \end{aligned} \tag{13}$$

Substitute (4) into (13) to get the non-linear equation of the system.

$$\left[J_s + J_p + \frac{1}{2}M_p(l+r)^2(1-\cos 2\theta_p)\right]\ddot{\theta}_p = \frac{nk_t}{R}(e_a - k_m n\dot{\theta}_p) - (l+r)\left[mg\sin\theta_p - \frac{1}{2}\rho A v^2(C_D\cos\theta_p + C_L\sin\theta_p)\right] - c\dot{\theta}_p \quad (14)$$

Linearizing equation (14)

$$f = \left[J_s + J_p + \frac{1}{2}M_p(l+r)^2(1-\cos 2\theta_p)\right]\ddot{\theta}_p - \frac{nk_t}{R}(e_a - k_m n\dot{\theta}_p) + (l+r)\left[mg\sin\theta_p - \frac{1}{2}\rho A v^2(C_D\cos\theta_p + C_L\sin\theta_p)\right] + c\dot{\theta}_p = 0 \quad (15)$$

Equilibrium conditions: $\theta_{p0} = 0$, $\dot{\theta}_{p0} = 0$, $\ddot{\theta}_{p0} = 0$, $e_{a0} = 0\ V$ and $v_0 = 0\ m/s$

$$f_0 = \left[J_s + J_p + \frac{1}{2}M_p(l+r)^2(1-\cos 2\theta_p)\right](0) - \frac{nk_t}{R}(0 - k_m n(0)) + (l+r)\left[mg\sin 0 - \frac{1}{2}\rho A(0)^2(C_D\cos 0 + C_L\sin 0)\right] + c(0) = 0 \quad (16)$$

The equilibrium conditions are suitable.

For linearization small angle approximations and the above equilibrium conditions were used

Term 1:

$$\left.\frac{\partial f}{\partial \theta_p}\right|_0 = (l+r)mg \quad (17)$$

Term 2:

$$\left.\frac{\partial f}{\partial \dot{\theta}_p}\right|_0 = \frac{n^2 k_t k_m}{R} + c \quad (18)$$

Term 3:

$$\left.\frac{\partial f}{\partial \ddot{\theta}_p}\right|_0 = J_s + J_p \quad (19)$$

Term 4:

$$\left.\frac{\partial f}{\partial e_a}\right|_0 = -\frac{nk_t}{R} \quad (20)$$

Term 5:

$$\left.\frac{\partial f}{\partial v}\right|_0 = 0 \tag{21}$$

Using Taylor series and perturbation theory the linearized equation of the system is

$$(l+r)mg\Delta\theta_p + \left(\frac{n^2 k_t k_m}{R} + c\right)\Delta\dot{\theta}_p + \left(J_s + J_p\right)\Delta\ddot{\theta}_p = \frac{nk_t}{R}\Delta e_a \tag{22}$$

Using Laplace transformations to move into the s-domain results in

$$\theta_p(s)\left[(l+r)mg + \left(\frac{n^2 k_t k_m}{R} + c\right)s + \left(J_s + J_p\right)s^2\right] = \frac{nk_t}{R}E_a(s) \tag{23}$$

Which is the system's transfer function.

4. Uncontrolled Plant Performance

4.1 Time Domain

In analysing the basic performance of both the non-linear and linear models, the time responses of both models were plotted for the free response, disturbance response and three different input signals [5][6]:

- Free-Response: this is the response of the system in the absence of an applied force or excitation (applied force in this case refers to the motor torque applied to the array by means of varying the motor voltage).
- Disturbance response: refers to the response of a system when the reference input is zero and the disturbance is non-zero.
- Step-Response refers to the response of a system to an excitation or input signal that instantaneously increases or decreases from some value to a different permanent value.
- Ramp- Response is the response of a system to a linearly increasing or decreasing input signal.
- Sinusoidal Response: is the response of a system to a smooth, wave-like function that oscillates continuously over time.

Time responses of both the linear and non-linear systems were plotted using from their respective block diagrams in Simulink. The various input signals modelled represent the motor input voltage, which in turn results in motor shaft torque, which through a worm-geared slew drive, results in output shaft torque that moves the solar array by some angle theta in degrees. For a complete system and the purposes of comparing the output rotation to the input, a potentiometer would be responsible for the conversion of rotation theta, to voltage for direct comparison. For the basic time performance this wasn't considered. However, given the driving motor has a voltage rating of 24VDC, analysis of the response assisted in the establishment of a mathematical relationship between the rotation theta in degrees and voltage in Volts for the potentiometer to be used for control purposes. The block diagrams for both the linear and non-linear models are provided in the Appendix.

4.1.1. Free Response

In the context of the solar panel array, 'free response' refers to the time-domain behaviour of the models when no external excitation (reference or disturbance) is acting on the system, i.e., when motor voltage is zero volts and permanently remains zero, and there are no wind loads acting on the array.

Considering the free response plot of both the linear (blue) and non-linear (red) models shown above:

Since the initial conditions of a panel imply a reference that is at rest (zero angular velocity, acceleration, and displacement), the angular displacement of both the linear system, theta, starts and remains zero degrees in perpetuity, this is due to the omittance of motor and wind-induced torque loads. whilst obtaining the linear system equation by linearising the non-nonlinear version. There is no reference or disturbance input, and consequently, in adherence to Newton's second law of motion, both array models remain in a state of rest.

4.1.2. Disturbance Response

For the solar array, disturbance response refers to the response of the system due to pressure or wind loads when the motor is not running (non-zero wind speed and zero input motor voltage). Depending on the magnitude and direction of the wind and or motor rotation, the behaviours of the linear and non-linear models may significantly diverge, thus making the non-linear approximation of the non-linear model irrelevant.

This response is useful in assisting the determination of the effectiveness of damping or breaking mechanisms (represented mathematically by damping constant c) when the motor is not running and cannot provide a holding torque. Use of insufficient damping and or the presence of gustier winds at higher speeds would create an unacceptable disturbance error at equilibrium (gap between the flat horizontal portions of the blue and red plots below), thus undermining tracking efficiency.

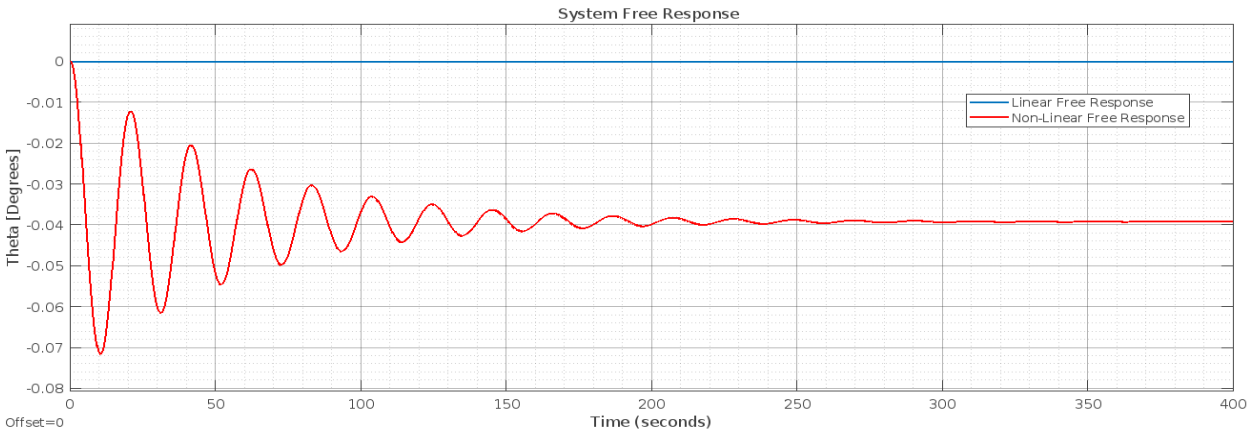

Figure 88:Free response for the uncontrolled linear and non-linear systems

As can be seen in the figure above, the linear response is zero because it is dependent only on the reference input and has 0 initial conditions about its equilibrium point. The Non-linear model, by contrast, results in a response characteristic of a second order system's step response. The response (angular rotation as a function of time):

- oscillates (an indication of the existence of non-zero imaginary parts in the roots of the non-linear model's characteristic equation)
- The oscillations decay (an indication of the presence of non-zero real parts of the system roots) in a seemingly exponential pattern with some time constant, this is also an indication of an underdamped system with complex roots.

The observed system oscillations dude to underdamping are manifestation of a transient response that requires improvement and optimisation.

4.1.3. Step Response

Both models were excited with step inputs of magnitude 1, 24 and –24. The respective magnitudes represent the magnitude of the input voltage supplied by the motor and as such step input of magnitude 1 represents increasing the input motor voltage from zero to 1V almost instantaneously. An input voltage of –24V results in the same output as that of a 24V input, albeit in the opposite direction (the motor can rotate both clockwise and counterclockwise or in reverse).

4.1.3.1. 1V Step Response

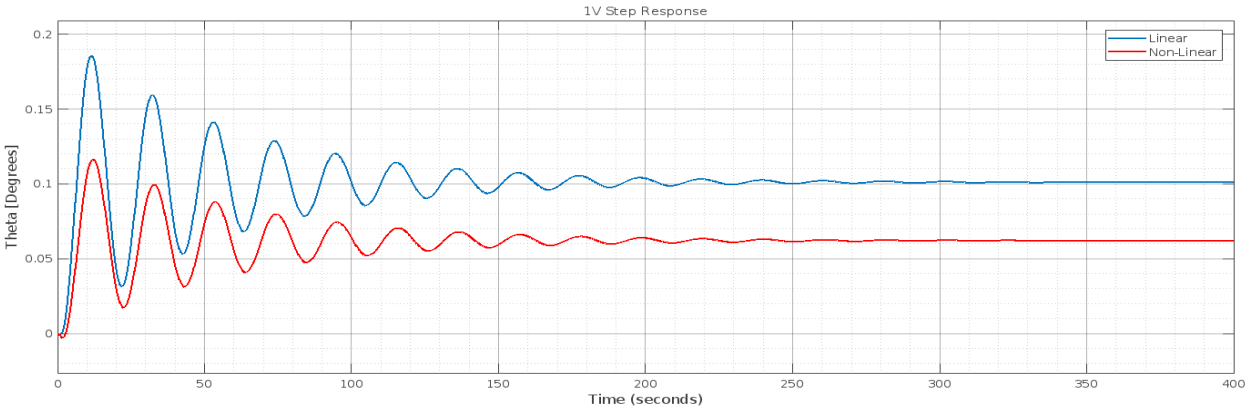

Figure 99: 1V Step response for the linear and non-linear systems

As can be seen in the plot above, the amplitude of the linear model is higher than that of the non-linear one for a 1V step input. This is because the non-linear system accounts for wind loads that result in a steady state offset of the array. For the simulated wind speed (6.5m/s) at time t=0s, the wind load displaces the array faster and more than the motor can provide a torque to move it to the desired position. Consequently, even though both models are displaced by the same angular rotation amount, they don't end up at the same position. The gap between the flat sections of both models (about 0.04 degrees for the plot above) is the steady state error in the linear response relative to the non-linear model.

The responses (angular rotation as a function of time) of both the linear and non-linear systems:

- oscillate (an indication of the existence of non-zero imaginary parts in the roots of each model's characteristic equation)
- The oscillations decay (an indication of the presence of non-zero real parts of the systems' roots) in a seemingly exponential pattern, this is also an indication of an underdamped system with complex roots.

Assuming the non-linear model is as close a representation of the real-life system as is possible, it is used in subsequent response analyses under this section as the benchmark against which the linear system is assessed.

4.1.3.2. 24V & -24V Step Responses

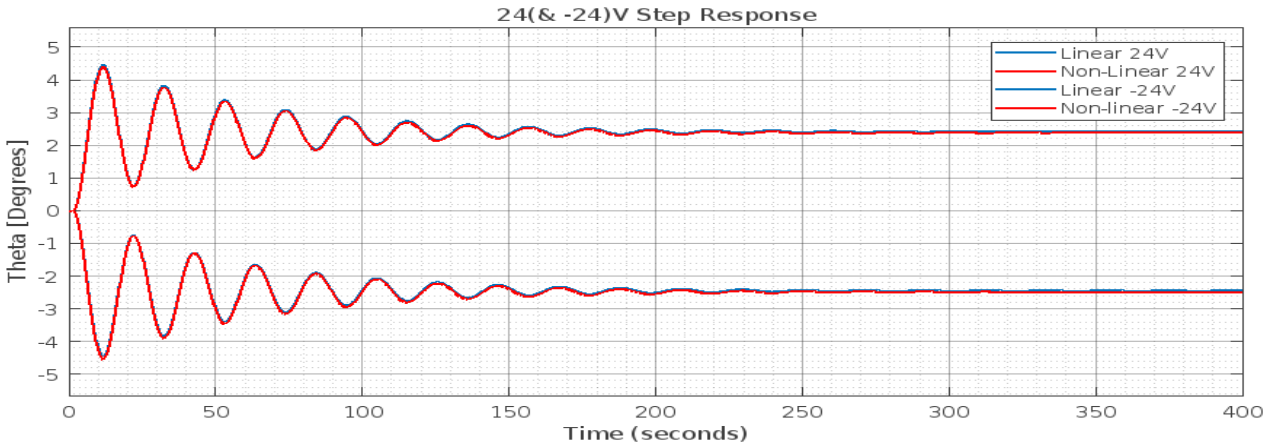

Figure 1010 24V and –24V step response for linear and non-linear systems

Consider the linear and non-linear responses to a 24V (rated motor voltage) step input plotted above. The general responses patten are akin to that of 1V step input: oscillatory and decaying, characteristic of an underdamped system with complex roots. The –24V response in this case is the same as its positive

counterpart albeit in the opposite direction. Due to the presence of wind loads in the non-linear model, the amplitude of the non-linear model is marginally lower than that of the linear model for positive motor rotation (against the wind) and marginally higher instead, for negative motor rotation (same direction as the wind).

Due to the increased driving input to the motor, the linear model is apparently a more accurate approximation of the non-linear system. This is because the torque produced by the motor is sufficient to almost nullify the wind loads produced by a wind speed of 6.5m/s. Therefore, the time domain performance of the open-loop linear model to an input step voltage of 1V can be summarised as follows:

- Rise Time: $t_r\ (10-90\%) = 0.44s$
- Settling Time: $t_s\ = 167.13s$
- Peak Time: $t_p\ = 1.31s$
- Max Overshoot: $M_p = 0.9768 = 97.68\%$
- Steady State-Error: 0 degrees

4.1.3.3. Small Angle Approximations: Divergence Of Linear Approximation from Non-Linear Model for Step Inputs of Varying Amplitude

One could conclude from the prior two subsections that increasing the amplitude of the step input (i.e., input motor voltage and consequently motor input torque) results in a more accurate linear approximation of the non-linear system. This is true but only to a given limit dictated by the assumption of small angle approximations.

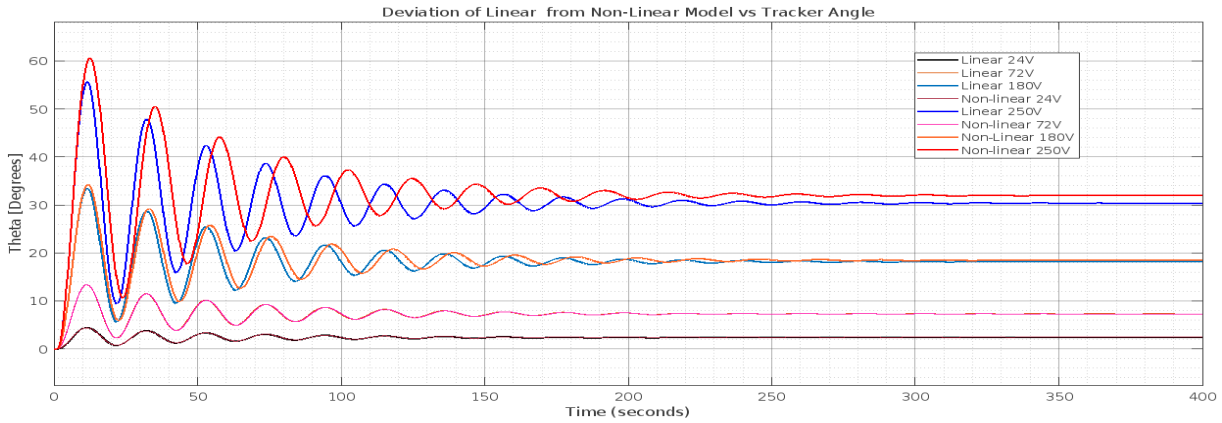

Figure 11:11 Comparison plot comparing linear system, non-linear system and desired tracking angles

Considering the plot in the figure above, it can be observed that there is barely a distinction between the linear and non-linear models for output angles less than 20-25 degrees. Larger angles due to increased amplitude of the step input (greater than approximately 25 degrees), however, result once more in a divergence between the linear approximation and the non-linear model (the first divergence being at very small step input amplitudes). Since the motor used in moving the array being modelled is rated at 24VDC, it is clear from the plot above that the assumption of small angles in the derivation of the linear model was a sound one since it is an accurate approximation of the more realistic non-linear system.

4.1.4. Ramp Response

In modelling the solar panel array, a ramp input implies the application of a voltage that linearly increases from zero at a constant slope (1V, 24V and -24V in this system).

4.1.4.1. 1V Ramp Response

Show in the plot below are the responses to a 1V ramp input. The initial oscillations in both ramp responses are a natural consequence of the system's response to a continuously increasing input. They are part of the transient response that eventually decays due to damping, leading to the system's steady-state behaviour of a continuously increasing output. The linear system behaves predictably albeit with potential for improvement of the transient response.

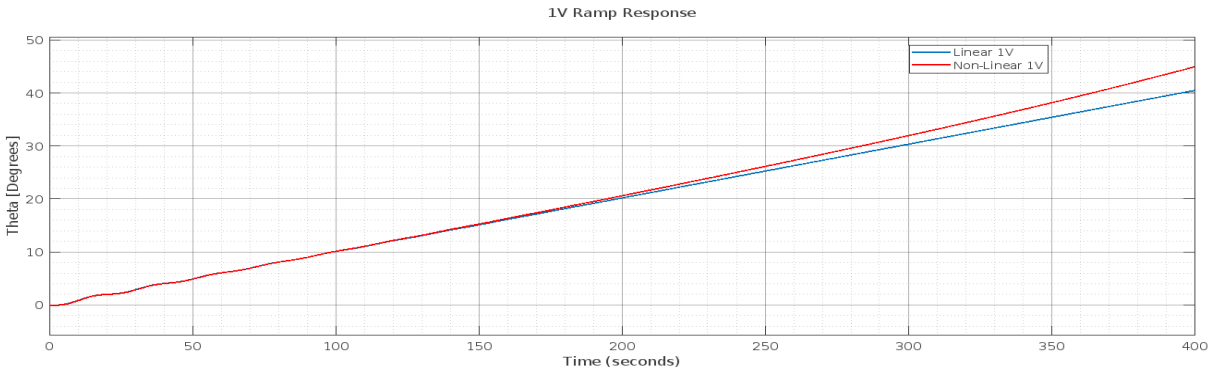

Figure 1212: 1V Ramp response for linear and non-linear systems

Like previous responses, the linear model provides an accurate approximation up to the limit of approximately 20-25 degrees (in accordance with small angle approximations), beyond which it diverges from the non-linear system. Due to fact that ramps increase in perpetuity, the system response is relevant only up to a given limit (20 degrees in this model), it is at this limit where a linear steady state error is measured.

4.1.4.2. 24V Ramp Response

The response to a 24V ramp input is also exponential albeit with a steeper slope or rate of change. Below are plots that show the response up the point of divergence of the linear approximation beyond small angles and the entire ramp response.

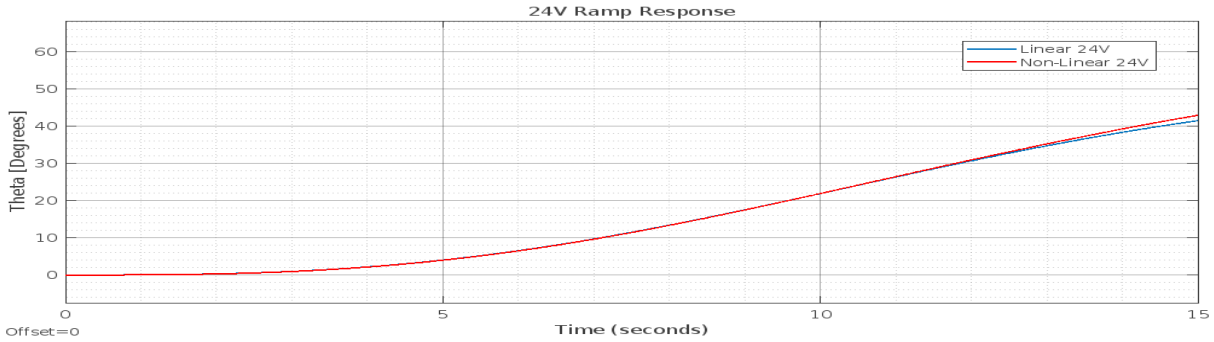

Figure 1313: 24V ramp response for linear and non-linear system for 15 s

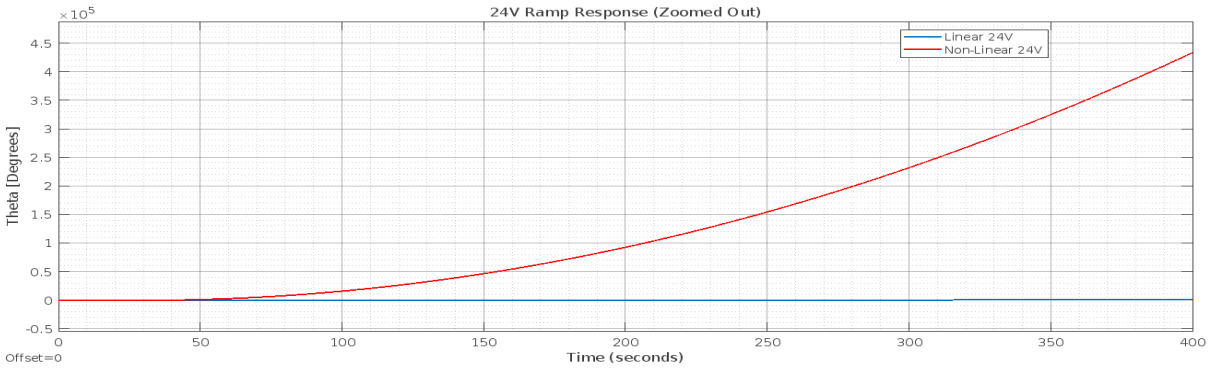

Figure 14:14 24V ramp response for linear and non-linear systems for 400 s

4.1.5. Sinusoidal Response

For the solar array, this refers to the constant alternating of the motor input voltage.

4.1.5.1. 1V Sinusoidal Response

Plotted below are the responses to a sinusoidal input of 1V. Like the step input, for small motor input voltage (torque), the linear approximation of the non-linear system is not accurate due to the opposing effect of wind loads on the non-linear system that are not modelled by the linear approximation.

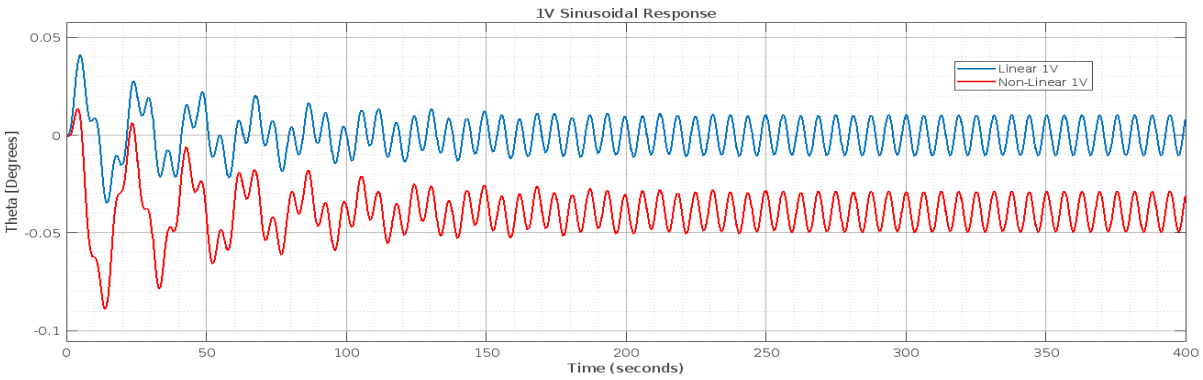

Figure 1515: 1V Sinusoidal response for linear and non-linear systems

The initially observed kinks that eventually dissipate or decay after approximately 150 seconds are characteristic of the transient response of the underdamped system being modelled. The eventual disappearance of the kinks is a good indication of favourable bounded stability behaviour of the system as opposed to them growing or persisting indefinitely.

4.1.5.2. 24V Sinusoidal Response

The response to 24V sinusoidal input is similar in structure to that of a 1V response, albeit the linear approximation of the non-linear system is more accurate. The system response, shown in the figure below, is as predicted, producing bounded output as a response to the bounded sinusoidal input.

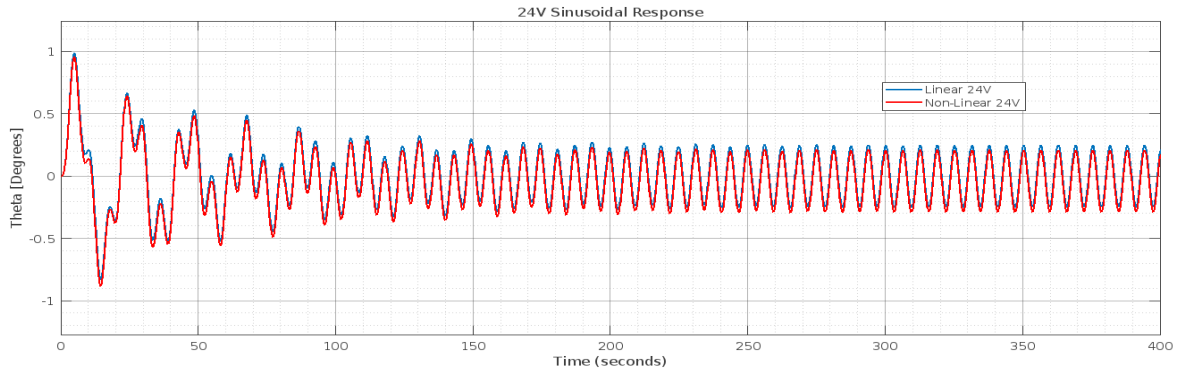

Figure 1616: 24V response for linear and non-linear systems

4.2. Frequency Domain

4.2.1. Frequency Response

The frequency response of a system is its steady state response to response to a sinusoidal input as "the input frequency is varied with time" [6].

4.2.1.1. Pole-Zero Plot

Information about the linear system's response and stability could be behaviour can be inferred from the pole-zero plot on the complex plane. Such a plot is shown below and plots the location of the system' zeros (values of s that make the linear transfer function equal to zero) and poles (values of s that make the transfer function go to the infinity, a singularity). The poles are marked with X's and the zeros with O's. As can be seen in the plot below marked by X, the two system poles are (-0.0180 + 2.2971i) and (-0.0180 - 2.2971i). Since the nature of the linear solar array model is of the standard transfer function form of a second order system with unity gain, the roots take on the form [6]:

$$s_{1,2} = -\xi\omega_n + i\omega_n\sqrt{1-\xi^2}$$

The pole-zero plot can be used to express key information about the system, namely the damping ratio z, and the natural frequency ω_n. These are shown on the provided plot:

- The poles are complex and thus suggest an oscillating system, damping ratio of 0.00781 suggests a severely underdamped system with excessive oscillation (as observed in the response plots in the previous section)
- natural frequency $\omega_n = 2.3\frac{rad}{s}$ and oscillation frequency at $\omega_d = \omega_n\sqrt{1-\xi^2} = 2.29\frac{rad}{s}$; the oscillation frequency being the same as the system's natural frequency means the system resonates.
- Response oscillations decay with time constant $\tau = \frac{1}{\xi\omega_n} = 55.67s$

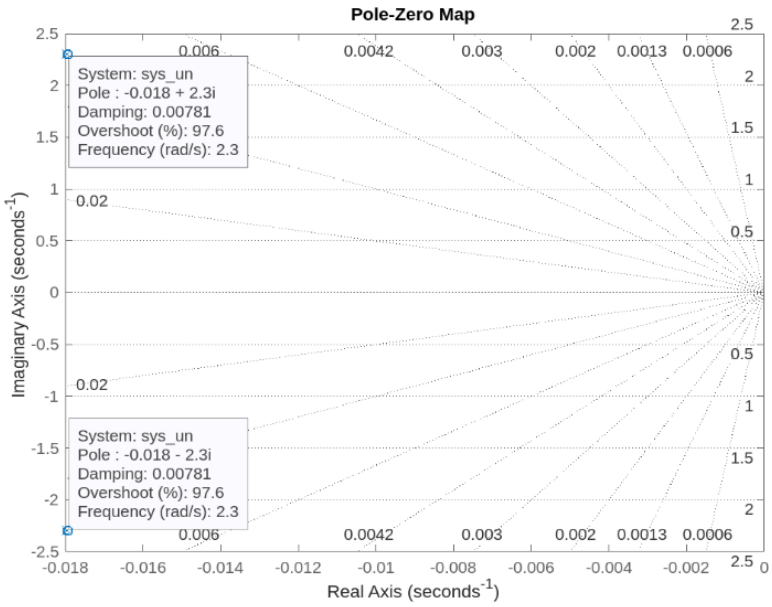

Figure 1717: Pole-Zero Map

4.2.1.2. Bode Plot

The bode plot show in the figure below, reaffirms findings made in the pole-zero plot regarding the resonant nature of the uncontrolled solar array model:

- The gain plot is at 0db for low frequency ranges; suggesting the system neither amplifies nor attenuates the input.
- The gain plot then rapidly increases towards, and peaks at a gain of approximately 36dB (input is amplified $M_p = 10^{\frac{36}{20}}$ = 63 times!) at an operating frequency of 2.29 rad/s (almost nearly the system's oscillation frequency of 2.3 rad/s)
- The gradual roll-off after the peak beyond 0dB suggests the system will attenuate higher frequency inputs.
- Reference trackers generally behave like low-pass filters [MATLAB], and this is confirmed by the Bode plot; there are two cut-off frequencies.

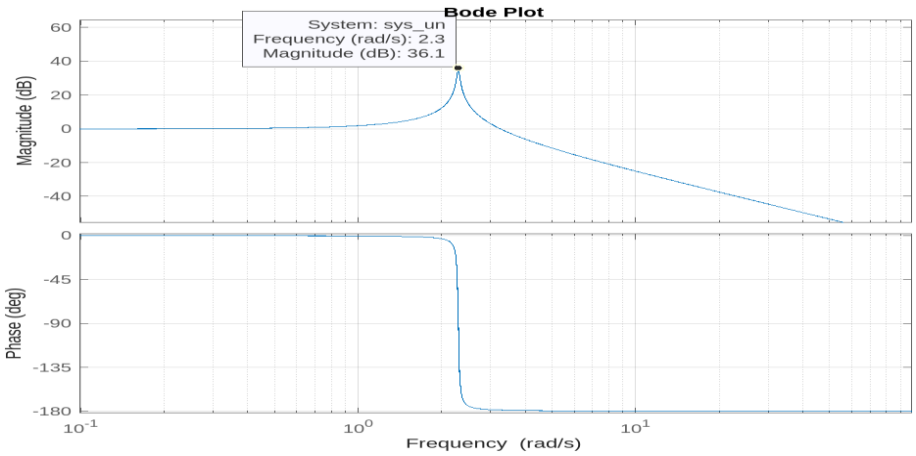

Figure 18:18 Bode Plot

5. Stability Analysis of Uncontrolled (Open Loop) Plant

5.1. Linear Stability

Numerous tools exist that are used to study the stability of a linear system, a critical component of this is determined in large part by the location of the poles of the characteristic equation.

5.1.1. Pole-Zero Stability

In addition to providing information about the response of a system, this method is used to infer stability information of a system from a plot of its poles and zeros on the complex plane as previously shown. The figure below shows the pole-zero plot of the roots of the characteristic equation of the linear solar tracker's equation of motion. Also plotted on the map is the overshoot, damping ratio and oscillation frequency of each of the system's two poles, whose roots are (-0.0180 + 2.2971i) and (-0.0180 - 2.2971i).

Strictly applying pole-zero stability theory to the two plotted poles, it can be concluded that the linear system is stable because the real parts of the roots of the characteristic equation are negative ($|\mathrm{R_e} = -0.0180$). This however, when considered with other criteria and response observations, is more likely to represent a system on the very brink of stability with marginal or limited stability ($i.e.,|\mathrm{R_e} = 0.0180 \approx 0$)

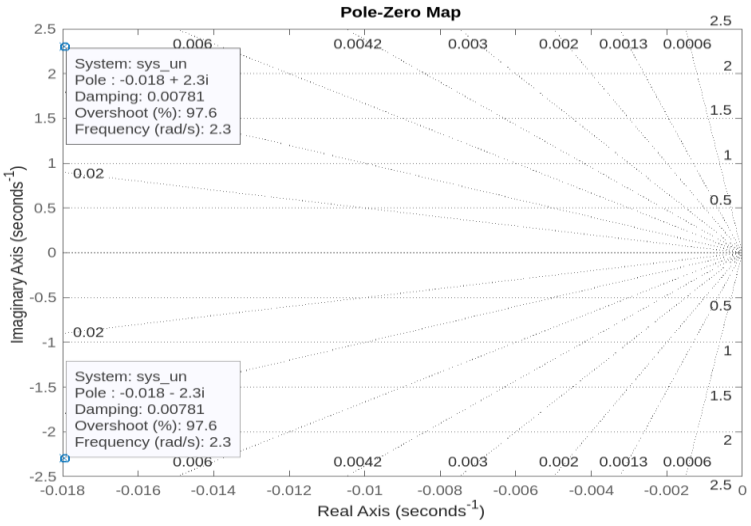

Figure 1919: Pole Zero Plot

5.1.2. Nyquist Stability

Applying the Nyquist stability criteria to the array equation the polar plots were generated, and the following observations made:

- The Nyquist plot does not enclose the point (-1,0*i*) and is shown on the zoomed in plot the right figure below.
- As shown in the Bode plot, the phase margin of the system (clockwise rotation of plot that cause enclosure with the point (-1, 0*i*)) is very small whereas no value of K (shifting of distance between plot real-axis intercept and origin) will cause the plot to enclose the point (-1, 0*i*)
- The plot never intersects the negative imaginary axis and thus the cutoff frequency cannot be extracted.

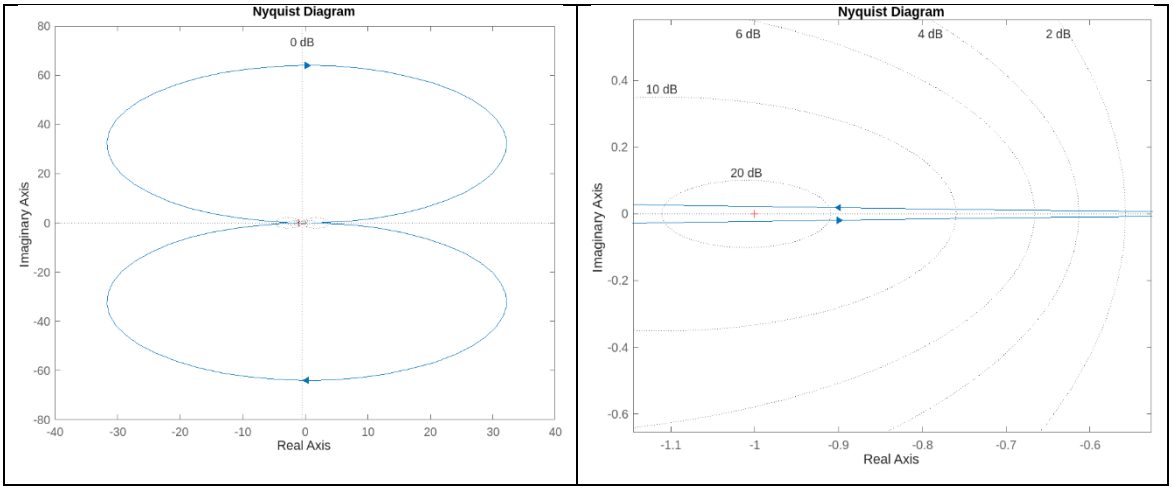

Figure 2020 Nyquist Plot

5.1.3. Bode Stability, Gain and Phase Margins

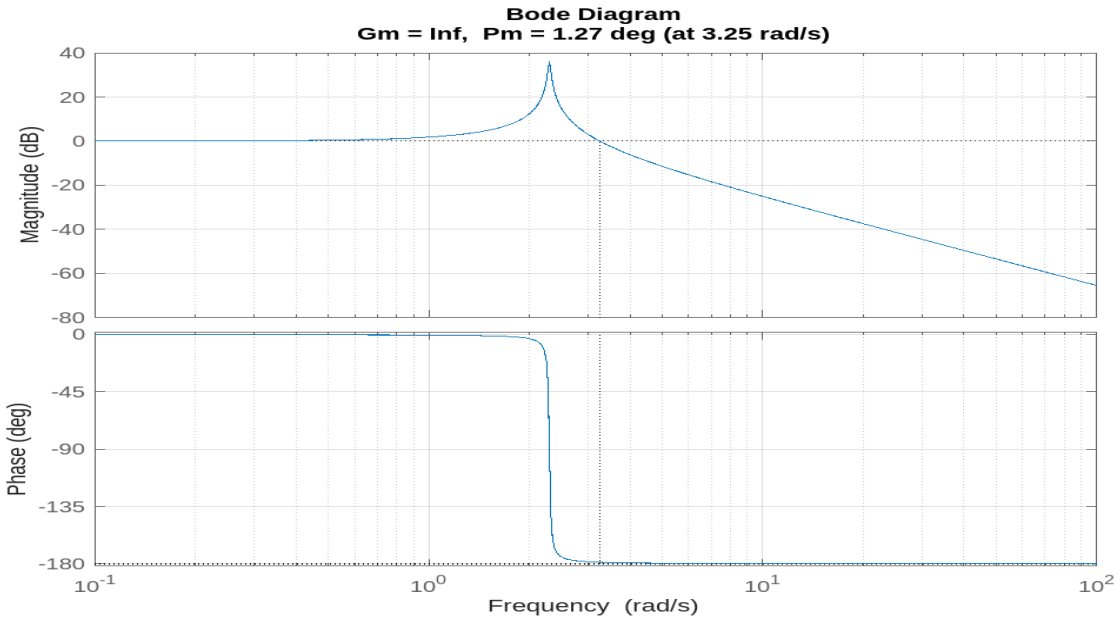

Figure 2121: Bode plot for the linear system

Considering once again the Bode plot of the linear equation, stability information can be extracted:

- Bandwidth = 3.5679 rad/s
- Gain Margin, GM = Infinite: This means the system will be stable for all values of gain K, (i.,e root locus plot does not intersect the imaginary axis), this is also implied by the fact that the phase plot asymptotes to -180 degrees and never crosses it (the system is never unstable over the all frequency ranges);
- Phase Margin, PM= 1.27 degrees: This result further evidences the neutral/marginally stable behaviour of the system, an allowance or phase margin of $1.27°$ (vs recommended PM $\geq 30°$ *or* PM $\geq 40°$) is on the brink of stability and the system could be very sensitive to parameter changes that potentially induce instability.
- Crossover frequency =3.25 rad/s
- The sharp peak in the gain plot and abrupt change in phase plot from zero rad/s to -180 rad/s at the frequency $\omega = 2.3\frac{rad}{s}$ suggest the system might be highly sensitive to parameter variation as this frequency [MATLAB].

5.1.4. Routh Hurwitz

The Routh Hurwitz table below was generated in MATLAB, and it indicates that the system is stable. The code is attached in the Appendix.

Table 2: Routh Hurwitz Table

```
 Routh-Hurwitz Table:
rhTable = 3×2
10^3  ×
      0.4116    2.1719
      0.0148         0
      2.1719         0

~~~~~> it is a stable system! <~~~~~

 Number of right hand side poles = 0



 Given polynomial coefficients roots :
sysRoots = 2×1 complex
    -0.0180 + 2.2971i
    -0.0180 - 2.2971i
```

5.2. Non-Linear Stability

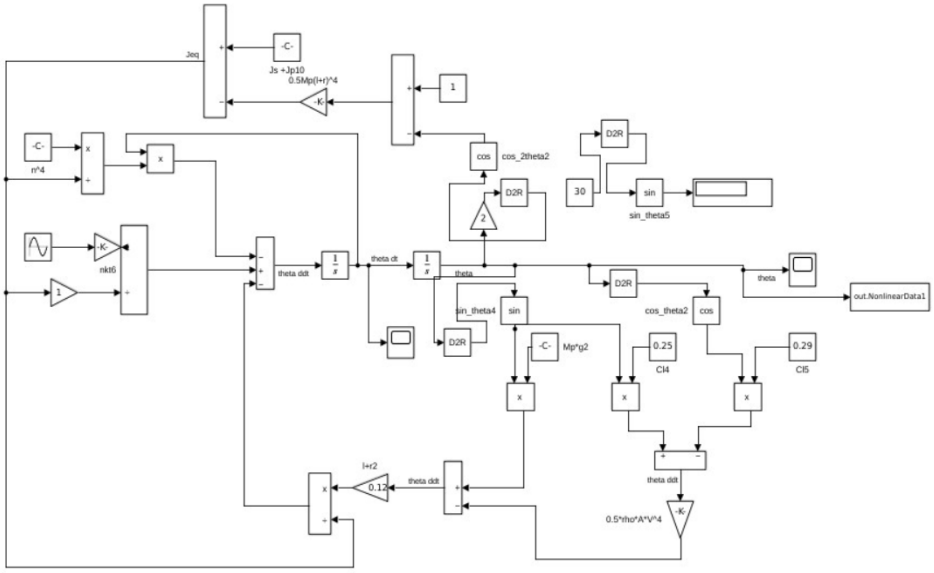

Figure 22: Non-linear Simulink Block Diagram

The non-linear system was excited with an impulse signal and its response plotted in the graph below.

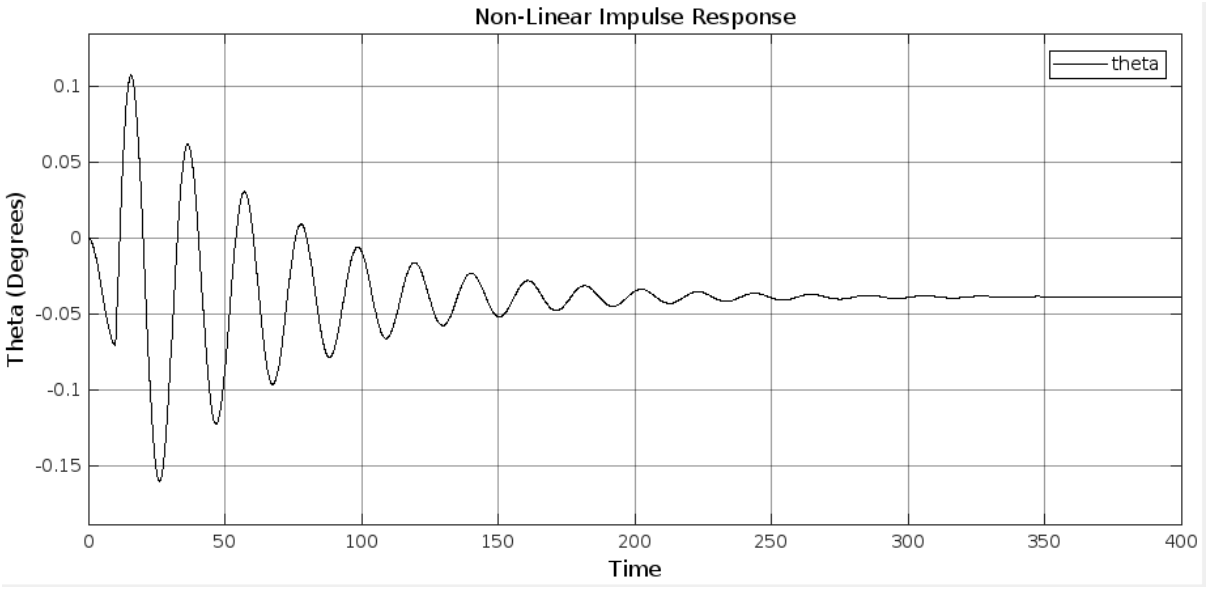

Figure 23: Non-Linear Impulse response

As can be seen, the plot resembles the step responses noted earlier. The system is excited from its equilibrium point at theta = zero degrees and the response oscillates until it eventually settles

permanently at a new stable equilibrium point. This behaviour is suggestive of a stable non-linear system since the perturbation motion does not persist indefinitely after the removal of the excitation, instead it completely dies out (decays).

Additionally, from observing the figure below, which shows the non-linear system's response to a sinusoidal input, it can be concluded that the non-linear system has BIBO stability. The response, as shown in the figure below, is bounded (restricted to some region defined by a sinusoidal function) in adherence to the applied similarly bounded input.

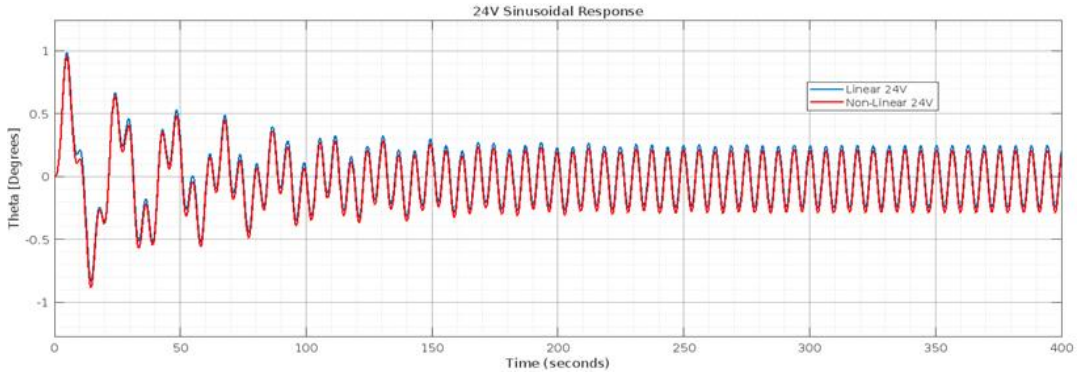

Figure 2324: 24V Sinusoidal response

When the system is excited by input signal that is subsequently removed, oscillations do not grow uncontrollably toward infinity as they would in an unstable system, nor does the system return to its equilibrium point as an absolute stable system would. The system does, however, settle at a new equilibrium point that is within a bounded region around the previous equilibrium point, suggesting the system is stable in the Lyapunov sense [6].

6. Controller Design, Analysis and Performance

6.1. Root Locus Technique

Root locus plot below was obtained using the rlocus function in MATLAB. The code can be found in the appendix. The plot shows the system is stable for all K values since no loci intersects the imaginary axis.

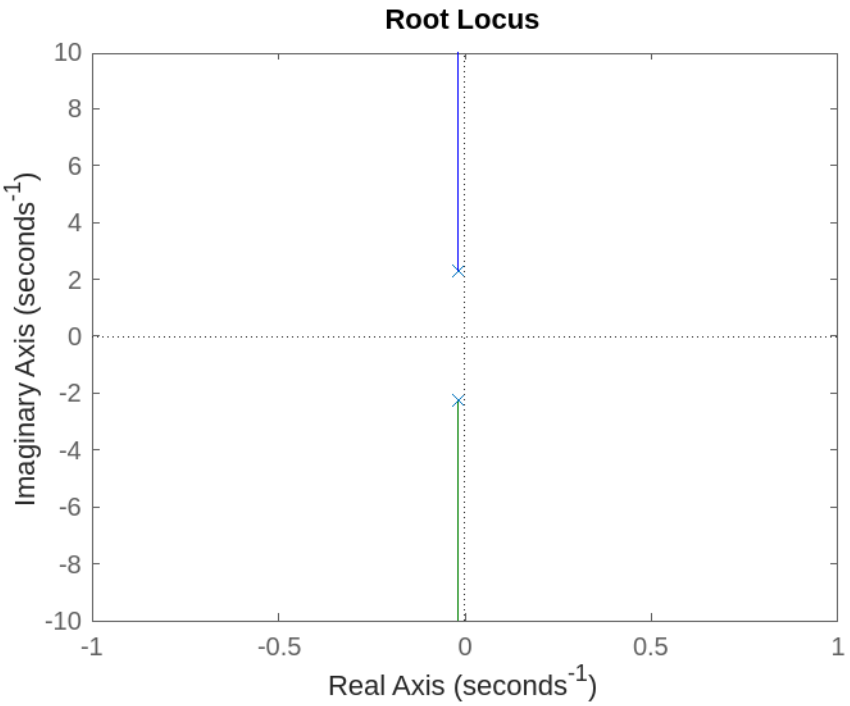

Figure 2425: Root Locus Plot

6.1.1. Analytical root locus

- Transfer function of the closed loop system is $T(s) = \frac{3.8502K}{411.59s^2+14.82s+2171.93}$
- Pole:$s_{1,2} = -0.0006486 \pm 2.297j$
- Zeros: None
- Both loci approach an asymptote.
- Asymptotic angles:

$$\theta = \frac{(2n+1) \times 180°}{P - Z}, \; where \; n \; = \; 0{,}1$$

For $n = 0,\ \theta = 90°$ and $n = 1,\ \theta = 270°$

- Asymptotic intersection points: $\sigma = \frac{\Sigma s_p - \Sigma s_z}{P-Z} = -\frac{-0.0006486+2.297j-0.0006486-2.297j}{2-0} = -0.0006486$
- Breakout point:

$$\frac{dG(s)}{ds} = 0 = \frac{K(0) - K(3.8502)(823.18s + 14.82)}{411.59s^2 + 14.82s + 2171.93}$$

- $s = -0.018$
- The root locus does not exist at this point. Therefore, we have no breakout points in out root locus, since every region has an even number of poles and zeros on either side.
- Angle of departure: $\theta_D = -\tan\left(\frac{2.297}{-0.0006486}\right) - \tan\left(\frac{-2.297}{-0.0006486}\right) = 0°$
- No Angle of arrival since we have no poles.
- We have no crossover value; therefore, we have an infinite number of K values that produces a stable system [7].

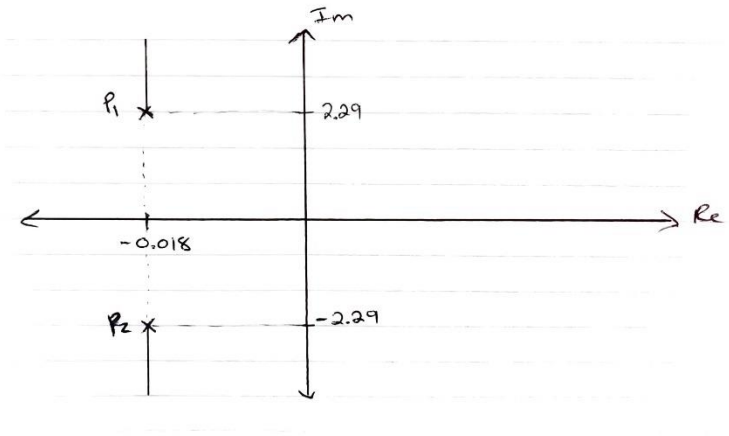

Figure 2526: Analytical Root Locus

6.2. PID controller: Proportional-Integral-Derivative (PID) Control Technique

To minimise oscillations and reduce the steady state error while maintaining stability, the solar tracker must implement a feedback controller. Several factors must be considered for selecting the type of PID controller that would be suitable for the purposes of simulating the solar tracker throughout operation throughout the day cycle, a 16-hour window is used to model the day in summer and 12 hours in winter, as seen in the figure below. The azimuthal angle of the sun at 30° latitude is used to simulate the solar position seen by an observer at that location. The system is modelled to move to the new solar position every hour to reduce power consumption. Among the various implementations of PID controllers, Proportional (P), Integral (I), Proportional-Integral (PI), Proportional-Derivative (PD), and Proportional-Integral-Derivative (PID), each offers distinct advantages and considerations [6][7][8].

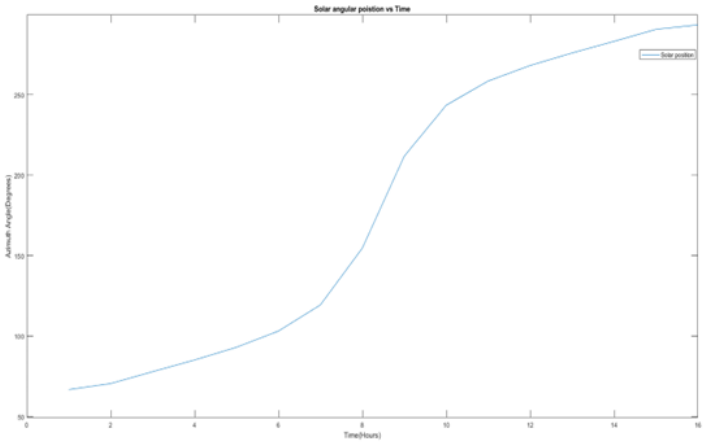

Figure 2627: Solar angular position during the day at the Kalkbut Farmhouse [9]

To determine the optimal PID controller type for a solar tracking application, several factors must be considered and evaluated including but not limited to the control objectives, performance specifications, and the physical dynamics of the system. Various PID subtypes were tested using a reference angle of 60° and a maximum input voltage of 24v for this system. MATLAB/Simulink's PID tuner was therefore used to tune and optimise the following gains for consideration [7].

6.2.1. P controller response

P type controllers generate a control signal proportional to the error, which is the difference between the reference value and the plant output feedback value, but making use of only a P controller may produce steady state errors which would be a continual offset between the desired angle and the output

angle across time. This persistent error never reaches zero identically, even if made arbitrarily close to the desired angle by varying the proportional gain.

The step response of the solar tracker to a proportional controller, which can be found in the Appendix, produced unstable results with high frequency oscillations for ramp, and step test inputs. The ramp angular response and voltage as a function of time, as seen below, produced approximately linear responses, but the angular response continually diverged from the reference input.

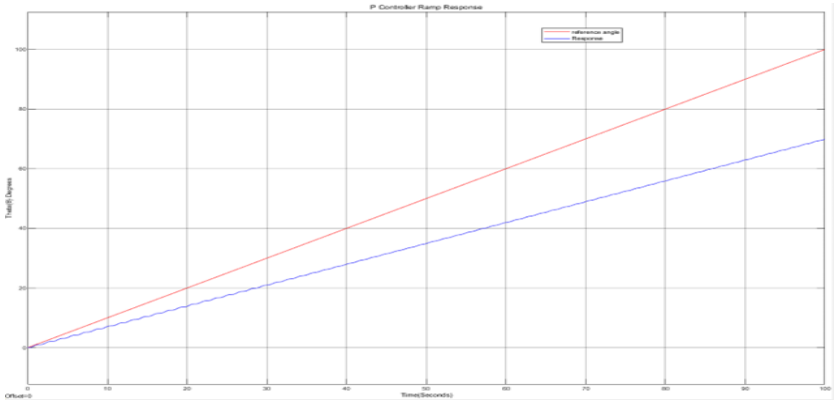

Figure 2728: P angular and voltage response graphs.

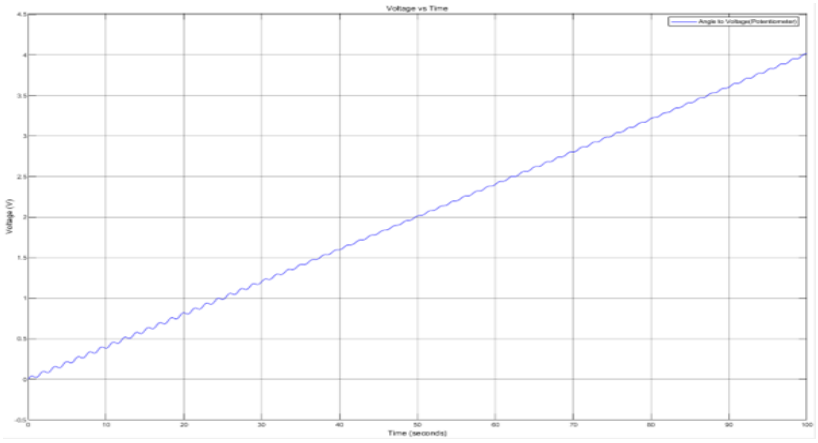

Figure 2829: P Controller angular and voltage response graphs.

The proportional controller fails to adequately meet the needs of the system, as seen in the step response in the Appendix, possibly due to factors such as mechanical inertia or vibration.

6.2.2. I controller response

The integral controller generates a control signal based over time based on the accumulated error by integrating the error signal over time. Using the Integral controller may help reduce steady state error by adjusting the signal to account for previous errors. The sole I controller produces a stable response.

For the ramp input but with a considerable angular error over 50 °, and a slow oscillatory response for the step input, which only reaches steady state after 300 seconds (5 minutes), but the high frequency oscillations are of considerable concern as high frequency oscillations reduce the operational life of the system. The increased steady state performance came at the cost of reduced transient performance.

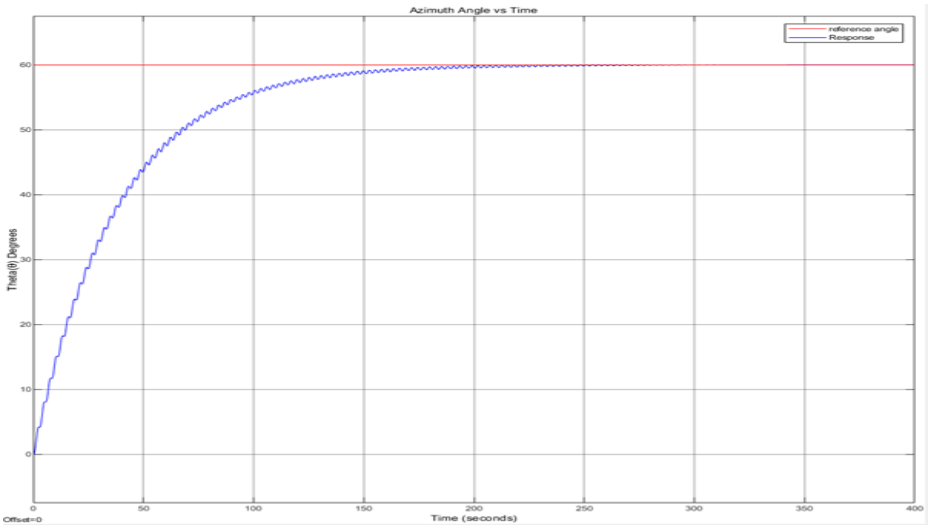

Figure 2930: I Controller Step Response

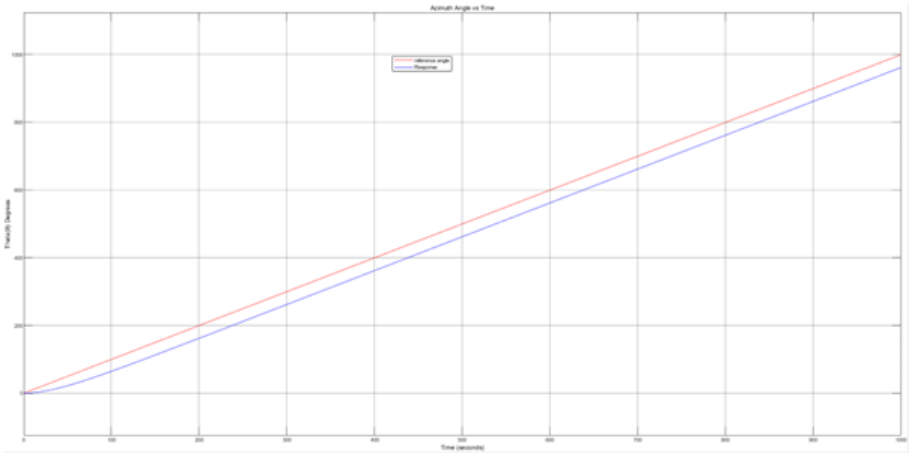

Figure 3031: I Controller Step Response

In Appendix A it can be observed that the I controller's response to a sinusoidal produces massive attenuation of the signal of approximately 90%. The step response performance is listed below in Appendix A.

6.2.3. D controller response

Derivative type controllers are never used by themselves, but in conjunction with other controller types. This is because derivative control signals have no effect on constant errors.

6.2.4. PI

Implementation of the PI control scheme produced similar results to that of the I controller with a higher attenuation of the reference signal for sinusoidal inputs of approximately, 97.5%, a higher steady state error for the ramp input of over 60°, a larger settling time of over 400 seconds. These response graphs are included in Appendix A along with their respective voltage responses. This is due to the fact the optimised PI gains calculated by Simulink produced a proportional $K_P = 0$ and reduced the Ki value from 1.9538 to 1.2328, as seen in Table 1 below, leading to reduced performance. The lack of proportional gain is unexpected and an avenue for future analysis and research.

Table 3: PI controller gains

Gain	P	I	D
Value	0	1.23285	0

Table 4: PI step performance

PI	
Steady-State Value (Degrees)	60 °
Steady-State Error (%)	0
Maximum Overshoot Value	60.303
% Maximum Overshoot	0.505
Peak Time(s)	0.247 s
Rise Time(s)	0.086 s
Settling Time(s)	1.5 s
Bandwidth	-

6.2.5. PD

A PD controller, which combined the proportional and derivative control actions, would theoretically reduce the error by responding to the current error deviation from the reference signal and the derivative control would respond to future errors by tracking the rate of change of the error, which would increase the damping if the oscillations and therefore improving the systems transient response performance.

However, given the solar trackers long operational time, where the dynamics are more predictable and slower, the transient response time is small relative to the entire operational time, improving steady state performance is judged to be of higher priority. Although there is improvement in the steady state error, the offset is still noticeable and diverges from the reference signal for large angular displacements. The PD controller gains are listed in Table 5.

Table 5: PD controller gains

Gain	P	I	D
Value	5144.289259	0	571.0210556

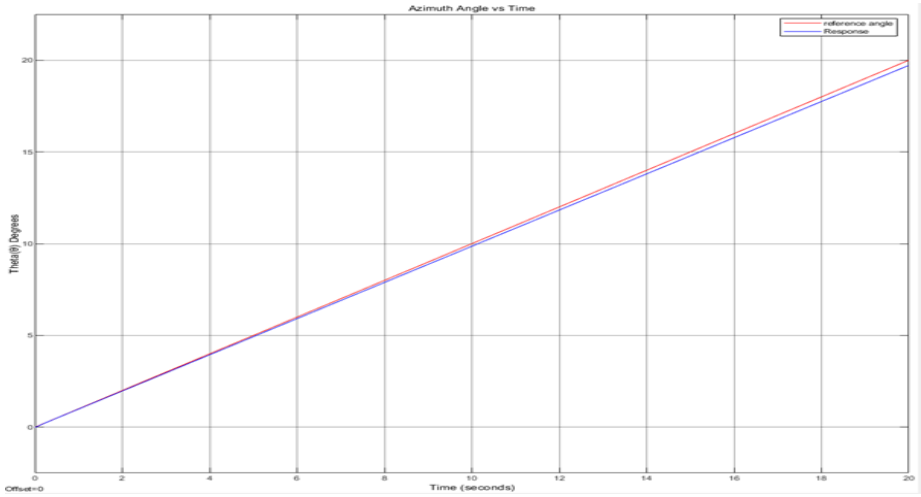

Figure 3132: PD controller ramp response.

The voltage response to a ramp input shows an overall steady increase in voltage, with a noticeable oscillation in the transient section of the response.

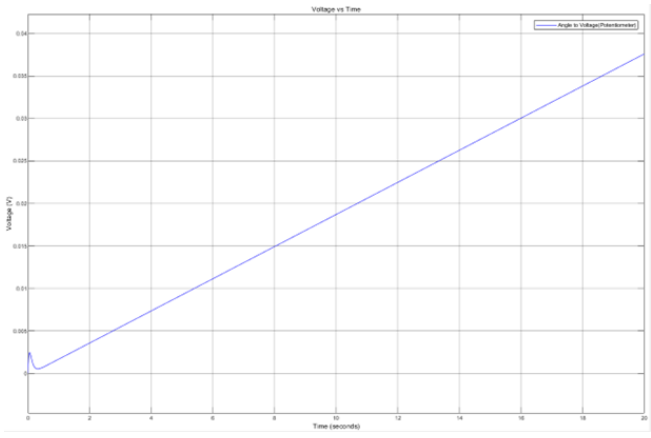

Figure 3233: PD Controller Voltage vs Time Ramp Response

The noticeable decrease in transient performance of the voltage vs time response for the sinusoidal and step inputs are included in Appendix A.

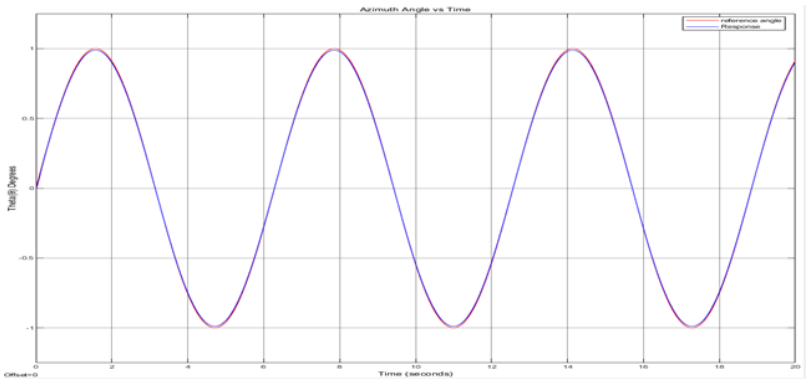

Figure 3334: PD Controller Sin Response

The sine response shows an improved response to unit sinusoidal inputs relative to earlier control schemes, with little to no attenuation of the input signal as well as zero phase shift.

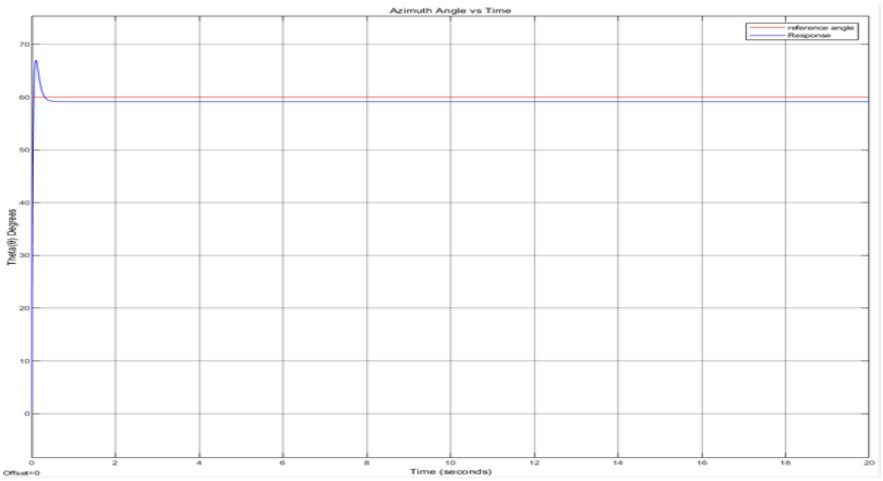

Figure 34: PD Controller Step Response.

The PD controller's response shows a to a 60° ramp input with a 13.07% maximum overshoot, but with less than a second rise time. However, there is a steady state error of 2.5%. The PD step response performance is summarised in Table 6, and the frequency response can be found in Appendix A.

Table 6: PD step response performance

PD	
Steady-State Value (Degrees)	60
Steady-State Error (%)	11.77%
Maximum Overshoot Value	67.04
% Maximum Overshoot	13.07%
Peak Time(s)	0.098
Rise Time(s)	0.035806
Settling Time(s)	0.525
Bandwidth (rad/s)	11.4

6.2.6. PID Controller

Finally, the PID controller combines all the controller responses to achieve precise control of dynamical systems. The integration of the PI controller assists in the reduction of constant deviation from the reference angle input setpoint, in this case the sun's angular position, thus gradually reducing the steady state error over time [8]. The addition of the D will help reduce transient error behaviour. As the sun's position changes with the season, using the D controller will help with the lack of predictability. The complete PID package, although more expensive, allows for control action based on past, current, and future errors, which ensures superior dynamic behaviour. This translates to faster settling times, reduced oscillations, stability, and overall improved dynamic behaviour at the cost of increased complexity and precise adjustment of the PID gains [6]. The controller gains attained are listed in the table below.

Table 7: PID controller gains

Gain	P	I	D
Value	1031.528257	1064.797	219.6043112

The PID controller's response to a ramp input shows essentially zero steady state error and transient effects such as initial oscillations or overshoot.

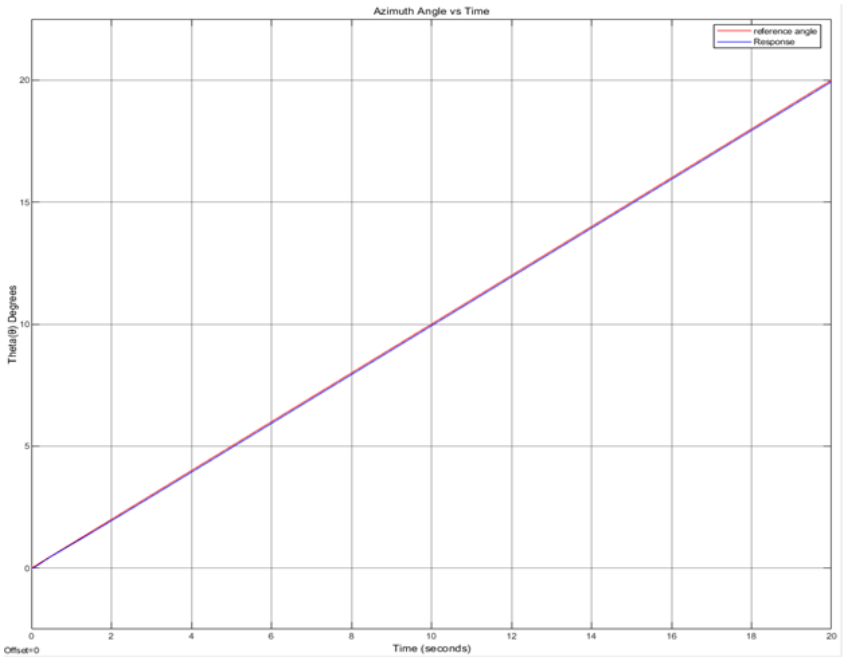

Figure 3135: PID Controller Ramp Response

This desirable response produces transient oscillations in the voltage response, probably a side effect of producing a high-quality response. The sinusoidal response shows no significant improvement over the PD controller, which both have minimal attenuation of the reference signal and zero lag in phase. The voltage responses are included in Appendix A, for completion.

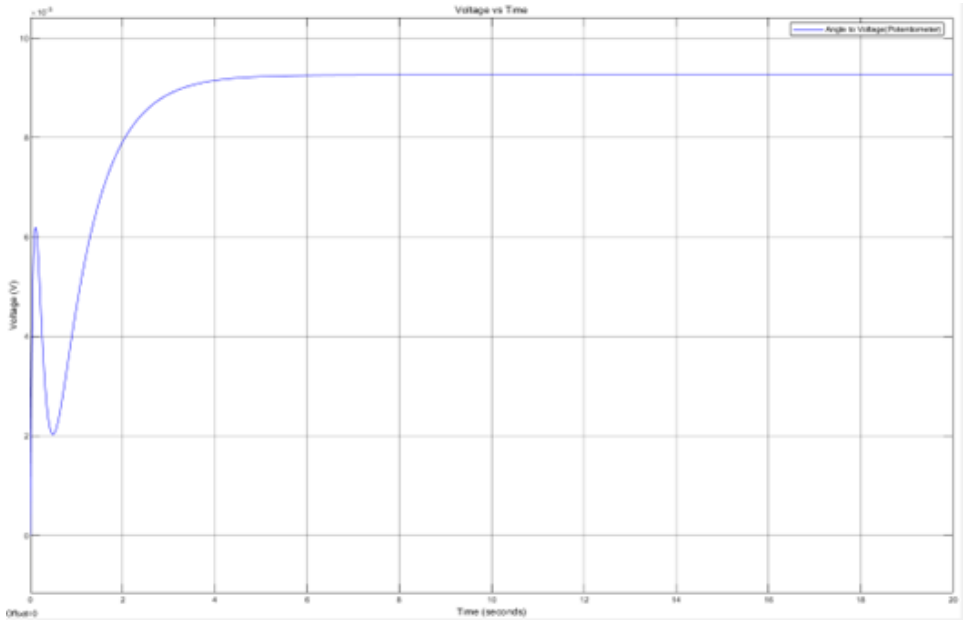

Figure 3236: PID Controller Voltage vs Time Ramp Response.

The step response of the PID controller to a 60-degree input angle, shows significant improvement over the PD controller design, particularly in the elimination of steady state error at the cost of increased settling time which is more than justified trade-off given the long operational time of the solar tracker.

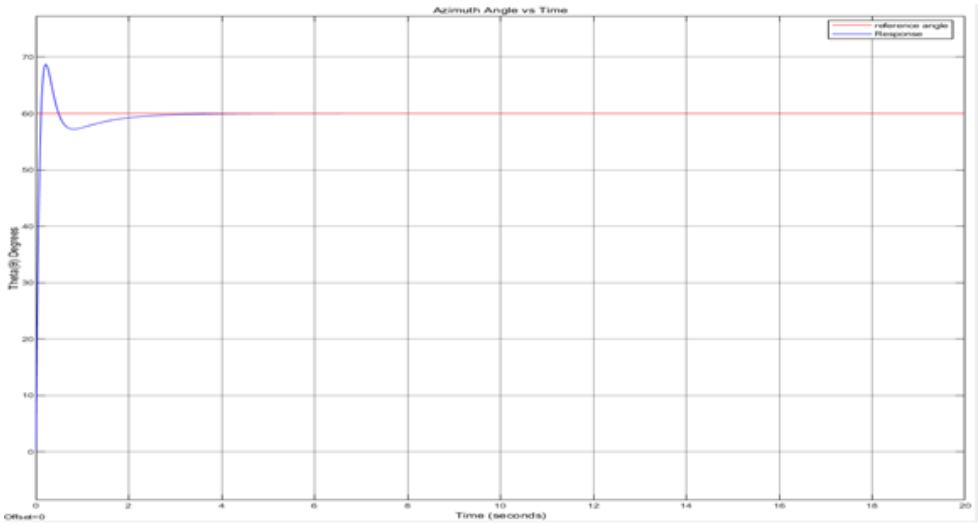

Figure 3337: PID Controller Step Response

The PID controller was selected over the preceding controller designs due to its superior ability to attenuate transient and steady state error, at the cost of an increase in maximum overshoot of just over 1% compared to the PD controller. The step response performance is summarised in the table below.

Table 8: PID step response performance

PID Performance	
Steady-State Value (Degrees)	60
Steady-State Error (%)	0.00%
Maximum Overshoot Value	68.6208
% Maximum Overshoot	14.53%
Peak Time(s)	0.212
Rise Time(s)	0.080432
Settling Time(s)	4
Bandwidth (rad/s)	9.6003

6.3. Controller Application to Solar Data

To evaluate the performance of the PID controller, data of the sun's azimuthal angle at 30° latitude for the summer and winter months was taken from sunearthtools.com [9].

6.3.1. Summer tracking response

The response curve of the system tracking the sun in summer is represented in the figure below, was scaled down over 20 seconds to better visualise the transient effects from rapid changes. It can be observed that the tracking behaviour produces zero steady state error after about 2 seconds of transient behaviour at 115.01 degrees with an overshoot of 12.82 % and an undershoot of 0.628% at 8 seconds when the sun is at an angle of 338.06 degrees respectively.

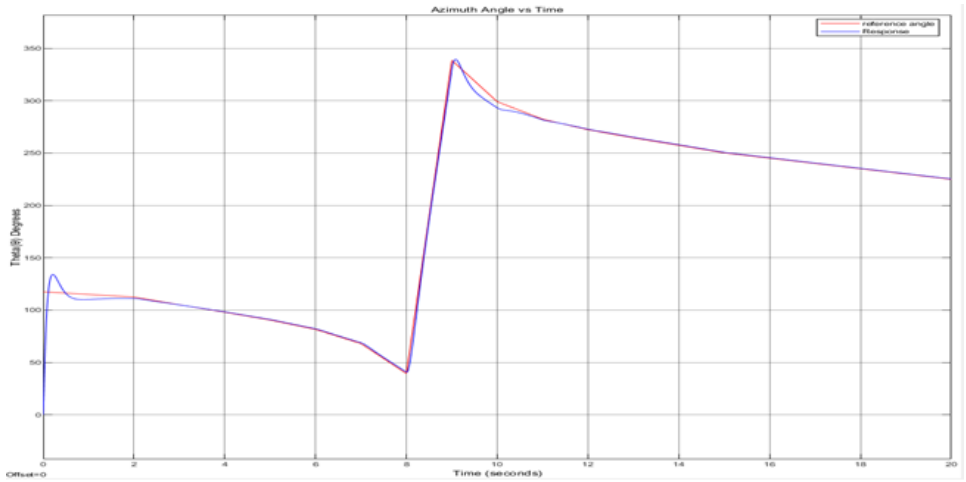

Figure 3438: System response curve of the system tracking the Summer solar azimuthal angle scaled from over to 16 hours to 16 seconds.

The response curve accurately scaled to simulate the response curve over 16 hours in the summer is shown in the figure shown below. It can be observed that at the scale of hours instead of seconds the transient effects are negligible.

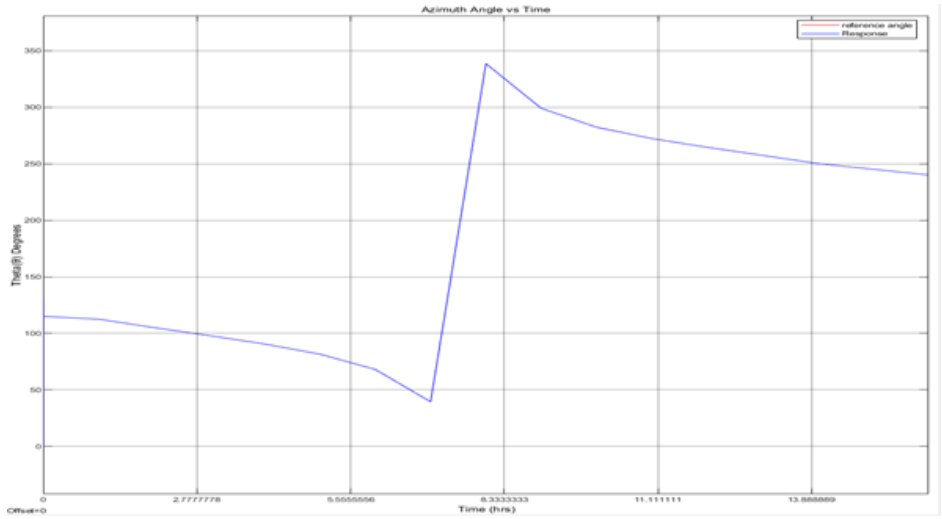

Figure 35:39 System response curve of the system tracking the summer solar azimuthal angle in hours.

6.3.2. Winter tracking response

From the winter solar data in the figure below, the hours of sunlight available are 12 which is less than that of the summer months of 16. Like the summer months there is noticeable overshoot of 8.152% at 62.52 degrees for approximately two seconds until settling time and again at 8 seconds but at a solar position 352.05 degrees with an undershoot of 2.428%. Otherwise, the system displays zero steady state error after the initial transient behaviour.

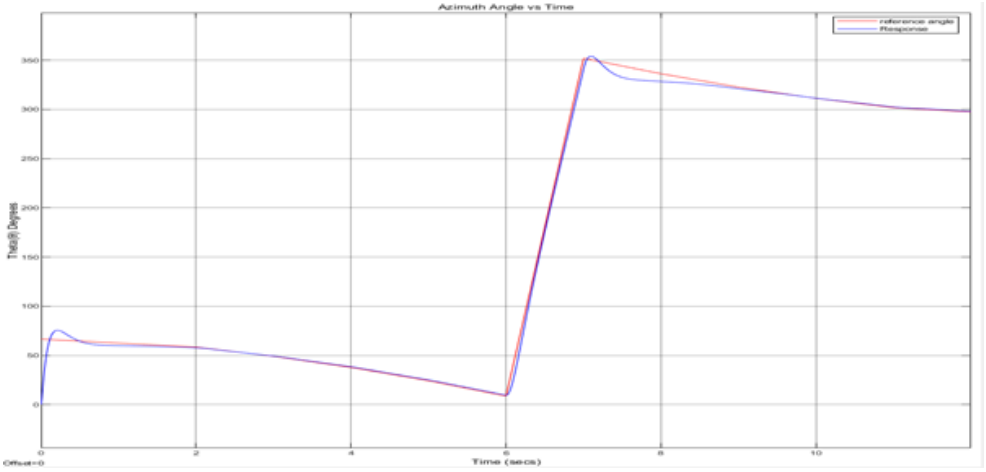

Figure 3640: System response curve of the system tracking the winter solar azimuthal angle scaled from over to 12 hours to 12 seconds.

Similarly, when the winter solar data is scaled realistically to track over hours, the transient effects observed at the start angle and 8 hours into the simulation are no longer observable.

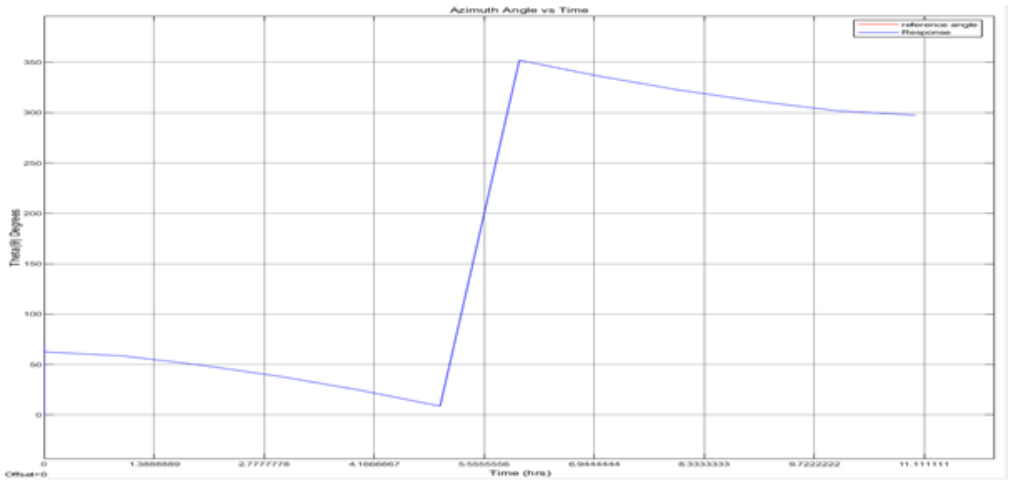

Figure 3741: System response curve of the system tracking the winter solar azimuthal angle in hours.

The MATLAB code, Simulink model and solar data sets are in the Appendix.

6.4. Instrumentation Required for Implementation

To implement the controller developed, the following hardware were identified [10][11].

6.4.1. Sun Position Sensors

Using various sensors such as Photodiode Sensors, Pyranometers or Light-dependent resistors (LDRs), the sun's position can be tracked by measuring the solar irradiance intensity, or by using solar position data.

6.4.2. Position Feedback Sensors

Position sensors such rotary encoders are needed to provide feedback on the angular position of the solar panel and are required to determine the error in the angle and the appropriate input signal to correct the position across time. Potentiometers can be used to convert the desired angle to an appropriate voltage as linear function between angle and voltage, essentially mapping the angular range of the panel to the voltage range provided by the motors.

6.4.3. Control Actuators

Servo motors offer high precision and control for closed loop systems such as solar trackers. They receive control signals from the PID controller and adjust the panels angular position according to the

error signal. Stepper motors are generally used for open loop applications and are suitable for fine adjustments in position.

6.4.4. Microcontroller or PLC

The microcontroller essentially serves as the brains of the system by processing signals between different components, logging data from sensors, and computing the required adjustment using a PID control algorithm. For these applications several options are available such as light weight systems such as Arduino boards, more complex systems such as Raspberry PI computing systems which has a more robust logging system. Alternatively, a PLC controller could be used for larger applications such as ours with a large array of panels to control, which is recommended.

6.4.5. Power supply

To provide regulated power to the system, a power system that includes a at minimum 24v battery system, with a regulation circuit (Buck/Boost converter) to provide consistent power and avoid fluctuations in power is required.

6.4.6. Communication interface

Reliable wiring between the sensors, controllers and actuators is required. Additionally, using a suitable communication protocol that allows for the required bandwidth of data to be sent and received should be considered. Wireless communication is a viable add-on to facilitate remote monitoring of the system and its data, as well as adjust systems operational parameters or update the code database without having to be on-site, would be advantageous.

6.4.7. Environmental Sensors

Sensors such as temperature sensors may need to be included to monitor environmental data to adjust the system's parameters to compensate for variations that might affect the sensor's calibration or the panel's efficiency. But most essentially, as far as sensors are concerned, a wind speed sensor, anemometers are required to allow the system to compensate for input disturbances, as well as adjust the panels position to ensure safe operation during high wind conditions to prevent damage.

7. DISCUSSION

The addition of the PID controller proved to be highly beneficial for the solar tracker system, significantly enhancing its performance in both the frequency and time domains, while effectively meeting the desired performance specifications.

In terms of steady-state error, the PID controller successfully maintained the system's error at 0%, indicating precise tracking of the sun's position throughout the day. This ensures that the solar panels are consistently aligned optimally, maximising energy capture.

The reduction in maximum overshoot from 97.68% to 14.53% is particularly noteworthy. This substantial decrease signifies improved stability and reduced oscillations in the system's response to changes in the sun's position. With an overshoot well below the 20% threshold, the system demonstrates excellent control over its movements, preventing excessive deviations from the desired trajectory.

Furthermore, the reduction in peak time from an uncontrolled value to 0.212 seconds, and the decrease in rise time to 0.08 seconds, indicate a significantly faster response to changes in sunlight direction. This rapid response enables the solar tracker to quickly adjust its position, ensuring minimal energy loss due to misalignment.

The most remarkable improvement lies in the settling time, which plummeted by 97.6% from 167.13 seconds to just 4 seconds under PID control. This dramatic reduction means that the system reaches its steady-state position much faster, minimising the time spent in transient states and maximising energy generation efficiency.

In the frequency domain, the PID controller enhanced the system's bandwidth, increasing it by almost threefold from 3.5679 to 9.6003 rad/s. This wider bandwidth allows the system to track changes in sunlight direction more effectively, enabling it to respond to higher-frequency variations with greater precision [6]. A summary of the system's performance relative to the desired performance specifications is summarised in Table 8, and the Improvement in performance of the controlled system relative to the uncontrolled system is detailed in Table 9.

Table 9: Summary of the performance specifications and the PID performance

Specifications performance	Desired Performance	Actual Performance
Steady-State Error (%)	0%	0.00%
% Maximum Overshoot	<20%	14.53%
Peak Time(s)	<2 seconds	0.212
Rise Time(s)	<1.8 seconds	0.080432
Settling Time(s)	<5 seconds	4
Decay ratio	<0.3	0.2354
Peak Amplitude ratio	1-1.5	1.145
Phase Angle	0	0

Table 10: Comparison of the uncontrolled and PID controlled performance specifications.

	Uncontrolled performance	PID Performance
Steady-State Error (%)	0	0.00%
% Maximum Overshoot	97.68%	14.53%
Peak Time(s)	1.31	0.212
Rise Time(s)	0.44	0.080432
Settling Time(s)	167.13	4
Bandwidth(rad/s)	3.5679	9.6003

The PID controlled systems performance when solar position data is used to test the system, showed promising results for both the summer and winter tracking scenarios. The performance specifications had to be modified slightly to better suit this application as the previous specifications did not translate automatically. The settling time for a solar tracker is interpreted as the time it takes for the system to stabilise and adjust after a significantly large change in angle, such as the initial angle at t =0, and at t = 8 seconds. The tracking during the summer settled after 2.5 seconds while the winter tracking fared better with a settling time of approximately 2 seconds.

The maximum percentage overshoot remains the same as the percentage it overshoots the requested angle before stabilising, and performed poorly during the summer simulation, with an overshoot above the performance specifications of less than 20% while the winter scenario fared better with an overshoot of 18.45%.

The tracking error is approximated as the steady state error for tracking a continuously moving target and is zero for both the winter and summer simulations. The response time is defined as how quickly the system can respond to gradual or instantaneous changes in the sun's angular position. This time however the summer scenario performed better.

Finally, the phase angle conceptually remains the same as the angular lag between the input reference angle signal and the angular response signal of the system. Here, both systems maintained a phase angle of zero, indicating good performance and stability.

Table 11: Performance indices for the summer and winter simulations.

Specifications Performance	Winter Tracking Performance	Summer Tracking Performance
Settling Time(s)	Approx 2 s	approx. 2.5 s
% Maximum Overshoot	18.45%	35%
Tracking Error %	0	0
Response Time (s)	0.67	0.44
Phase angle	0	0

The PID controllers' performance is evaluated here using numerous performance indices, listed with their values in Table 10, below.

Table 10: Performance indices for the summer and winter simulations [6][12].

Performance Indices		
Indices	**Summer**	**Winter**
IAE	0.6596	0.6918
ISE	0.1833	0.04145
ITAE	4.099	10860
ITSE	0.3544	0.9678

During the summer months, the solar tracker forms well according to the performance indices for a PID controlled system. The Integral Absolute Error (IAE) value was found to be 0.6596 which indicates that the tracker controller produces a small cumulative error over the course of the tracking period, which demonstrates effective error correction in the short term [6][12]. The Integral of Squared Error (ISE) value of 0.1833 reflects that large errors are not common and well-compensated for, which implies the system addresses any significant deviations from the reference relatively quickly. The Integral of Time-weighted Squared Error (ITSE) of 0.3544 corroborates this finding by indicating that any errors are both infrequent and short-lived. Overall, the low values across these metrics highlight that the PID controller effectively minimises errors, resulting in precise and stable solar tracking during the summer. Lastly, The Integral of Time-weighted Absolute Error (ITAE) of 4.099 shows that transient errors are corrected promptly, preventing them from persisting and thus ensuring efficient tracking. Continued fine-tuning of the PID parameters and regular system maintenance should maintain or further improve this performance [8].

However, the winter performance indices indicate several possible challenges for the controller. The IAE of 0.6918 remains low, indicating a generally well-performing system in terms of cumulative error. However, the lower ISE of 0.04145 suggests fewer large deviations, yet the remarkably high ITAE value of 10860 points to significant issues with constant cumulative errors in the system. This high ITAE implies that errors remain uncorrected for longer periods, likely due to the more difficult tracking conditions in winter, such as lower solar angles and shorter daylight hours. The ITSE of 0.9678, while higher than in summer, confirms that these persistent errors are indeed substantial and frequent [12]. To address these issues, seasonal tuning of the PID parameters is crucial, ensuring the system adapts to the different solar paths and environmental conditions. Steps suggested would be improving the tracking algorithm in a way that it can more accurately predict and adapt to winter conditions, servicing mechanical components for cold weather maintenance, and maybe integrating more environmental sensors onto the system. These enhancements are not expected to completely resolve all identified issues, but they will reduce them; consequently, solar tracking during winter will be more dependable and precise.

REFERENCES

[1] Karoospace. (n.d.). Solar Karoo. Available: https://karoospace.co.za/solar-karoo/

[2] Lane, C. (2021, March 27). What Is A Solar Tracker And Is It Worth The Investment? [SolarReviews]. Available: https://www.solarreviews.com/blog/are-solar-axis-trackers-worth-the-additional-investment

[3]Premium motion: Slew drive (2022) YouTube. Available at: https://www.youtube.com/watch?v=7Va-VnjCeeM (Accessed: 3 May 2024).

[4] Basilio, Joao & Moreira, M.V.. (2004). State–Space Parameter Identification in a Second Control Laboratory. Education, IEEE Transactions on. 47. 204 - 210. 10.1109/TE.2004.824846.

[5] Alan V. Oppenheim, Alan S. Will sky, and Ian T. Young. Signals and Systems (2nd Edition). Upper Saddle River, NJ, USA: Prentice Hall, 1997. [Online]. Available: https://www.pearson.com/en-us/subject-catalog/p/signals-and-systems/P200000003155/9780138229429]

[6] Palm, W.J. (2000) Modeling, analysis, and control of Dynamic Systems. New York: John Wiley & Sons.

[7] Pidtune, Tune PID controllers - MATLAB. Available at: https://www.mathworks.com/help/control/ref/pidtuner-app.html (Accessed: 17 May 2024).

[8] 'PID controller design for Complex Systems' (2020) PID Control System Design and Automatic Tuning using MATLAB/Simulink, pp. 233–258. doi:10.1002/9781119469414.ch8.

[9] info@sunearthtools.com. (n.d.). Calculation of sun's position in the sky for each location on the earth at any time of day [en]. https://www.sunearthtools.com/dp/tools/pos_sun.php?lang=en

[10] Ruelas Ruiz, José Efren & Muñoz, Flavio & Lucero, Baldomero & Palomares, Juan Enrique. (2019). PV Tracking Design Methodology Based on an Orientation Efficiency Chart. Applied Sciences. 9. 894. 10.3390/app9050894.

[11] Amelia, A. R., Irwan, Y. M., Safwati, I., Leow, W. Z., Mat, M. H., & Rahim, M. S. A. (2020). Technologies of solar tracking systems: A review. IOP Conference Series: Materials Science and Engineering, 767(1). https://doi.org/10.1088/1757-899X/767/1/012052

[12] Hanwate, S.D. and Hote, Y.V. (2018) 'Design of PID controller for Sun Tracker system using QRAWCP approach', International Journal of Computational Intelligence Systems, 11(1), p. 133. doi:10.2991/ijcis.11.1.11.

APPENDIX

A. Additional response Graphs for different controller schemes

1. P controller angular and voltage response graphs

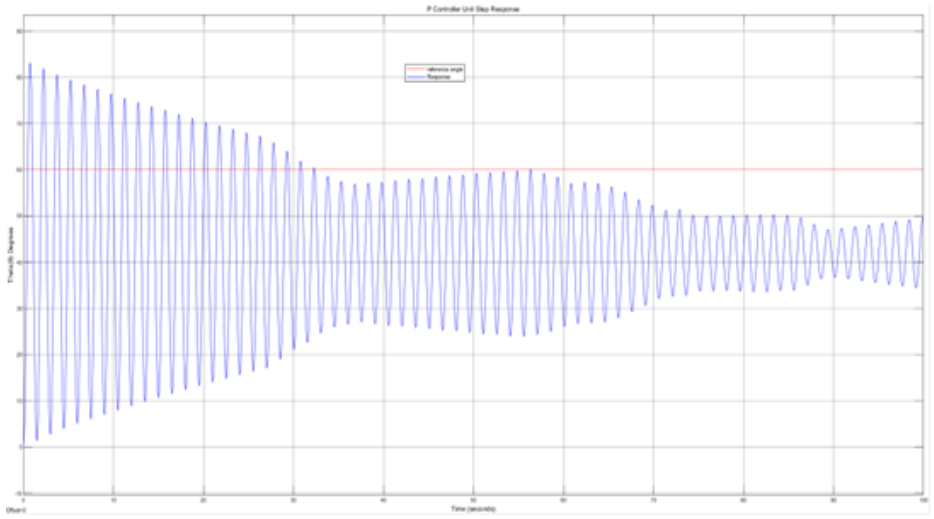

Figure 38 42: P Controller Step Response

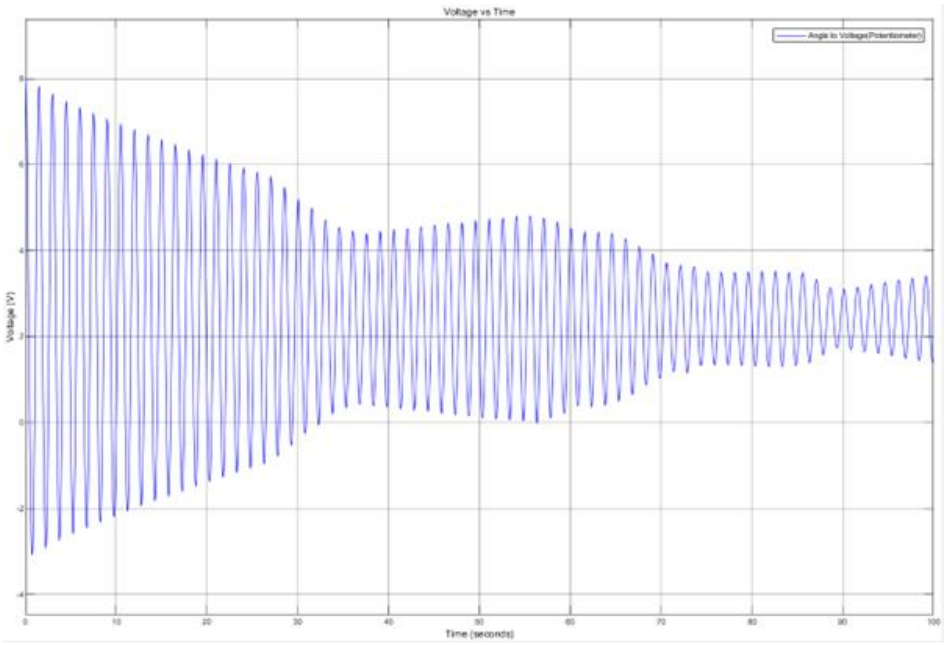

Figure 3943: P Controller Step Voltage Response

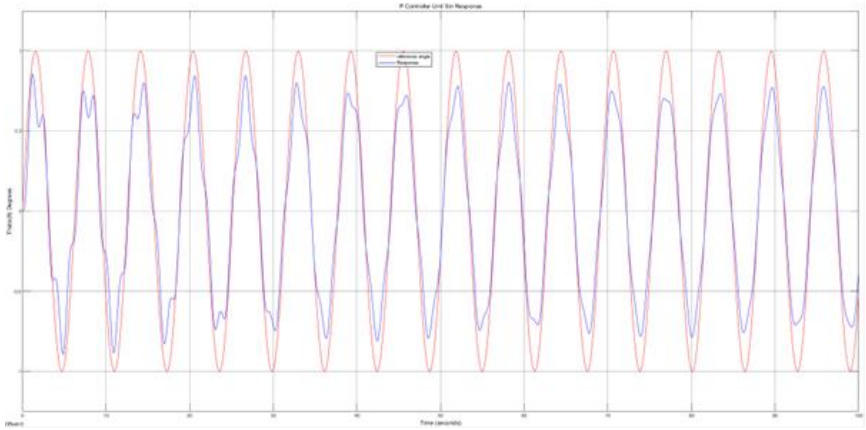

Figure 4044: P Controller Sin Response

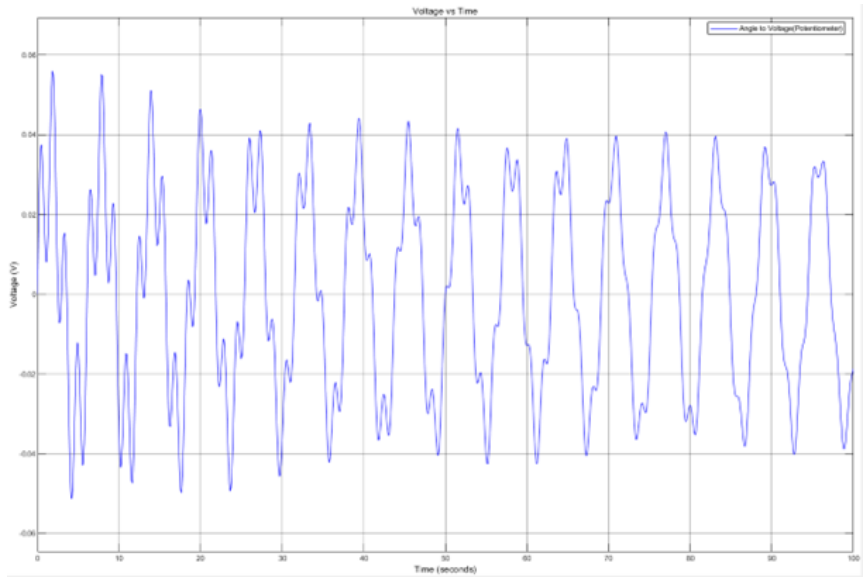

Figure 41:45 P Controller Sin Voltage Response

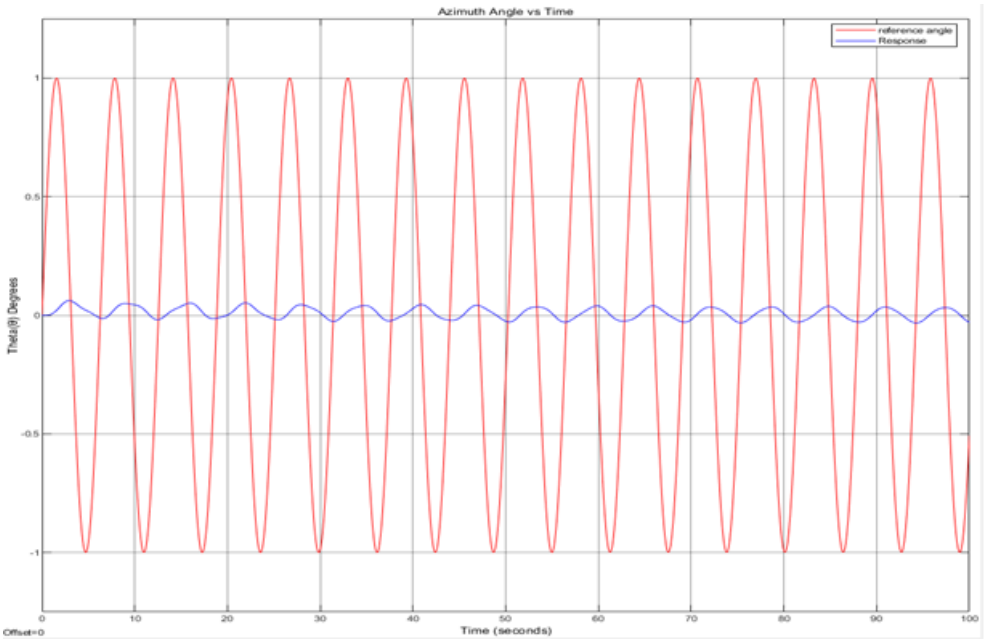

Figure 4246: I Controller Sin Response

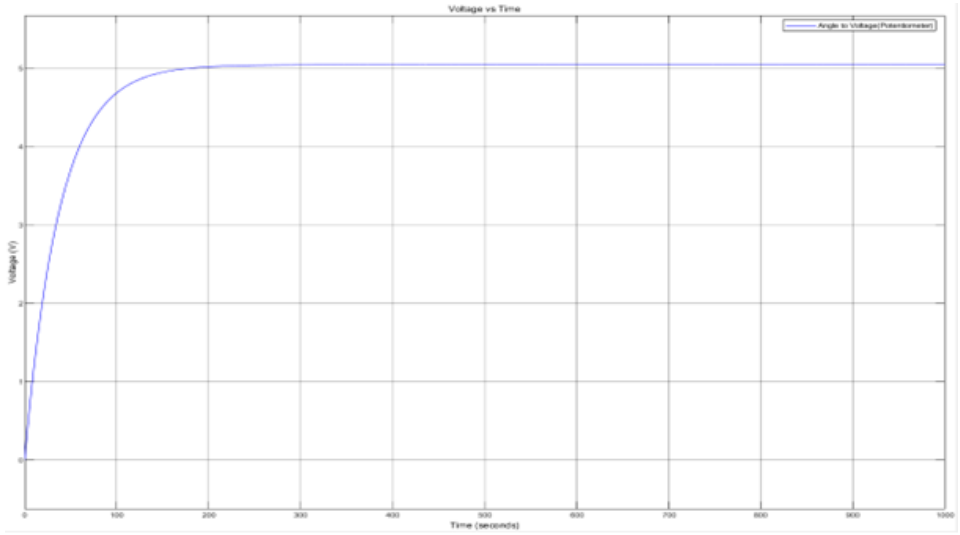

Figure 4347: I Controller voltage Step response graphs

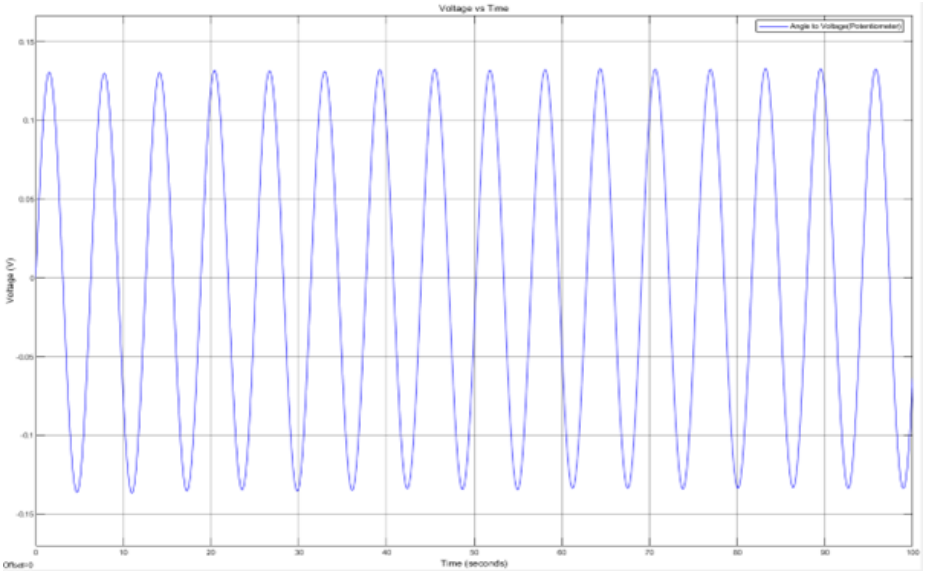

Figure 44:48 I Controller voltage vs Time Sin response graphs.

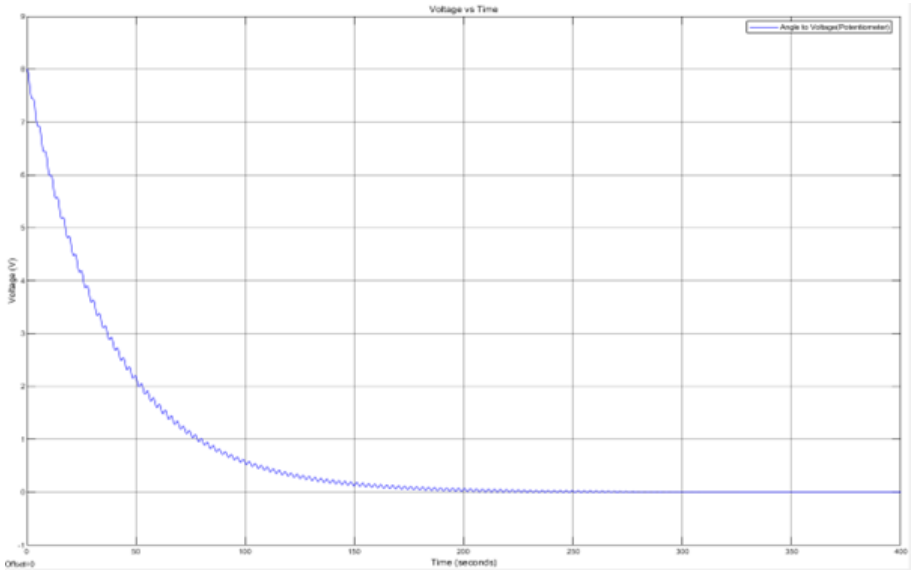

Figure 4549: I Controller Step Voltage Response.

2. PI angular and voltage response graphs

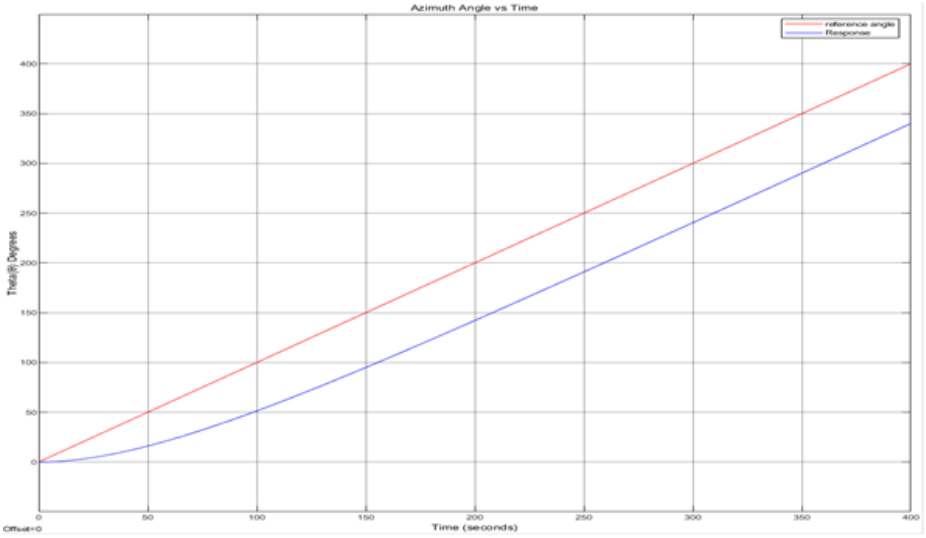

Figure 4650: PI Controller Ramp Response

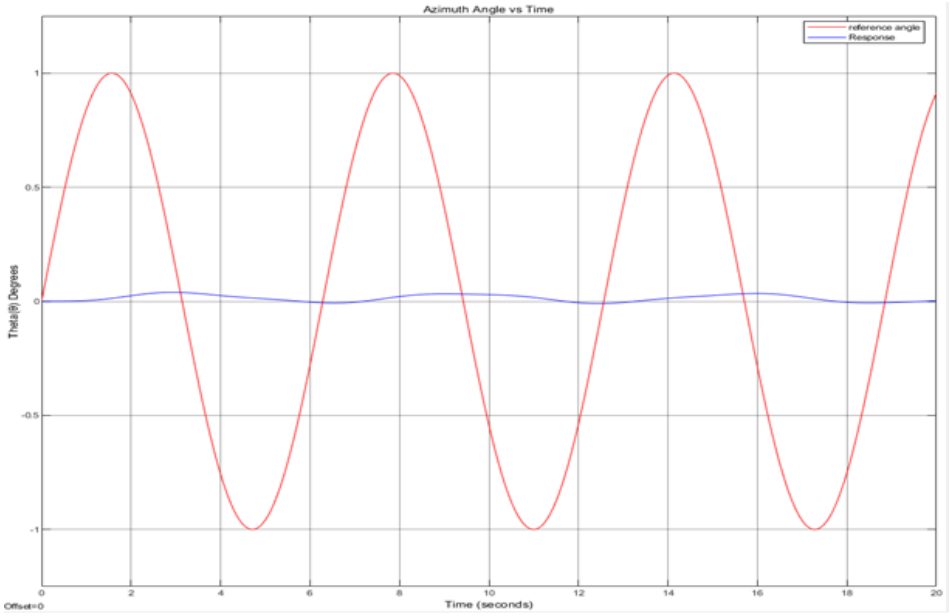

Figure 4751: PI Controller Sin Response

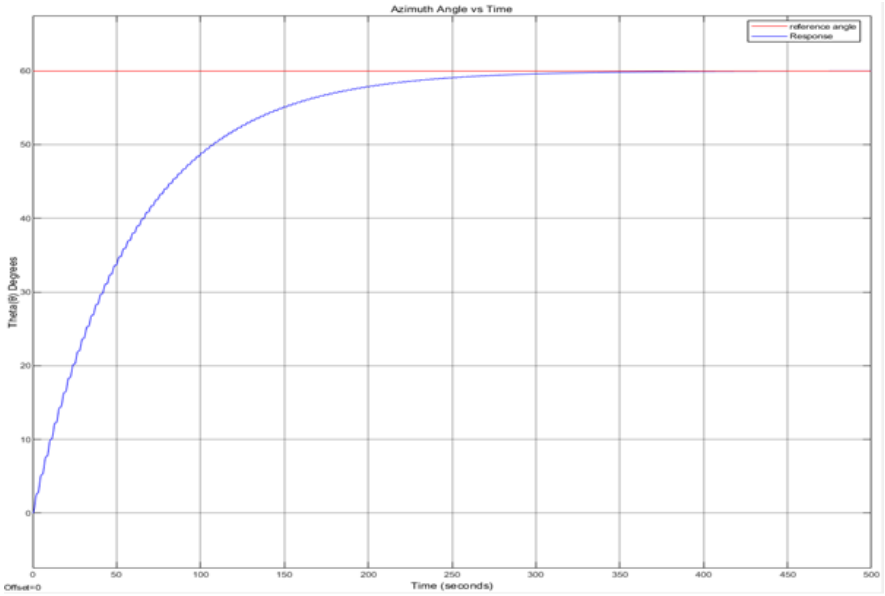

Figure 4852: PI Controller step Response.

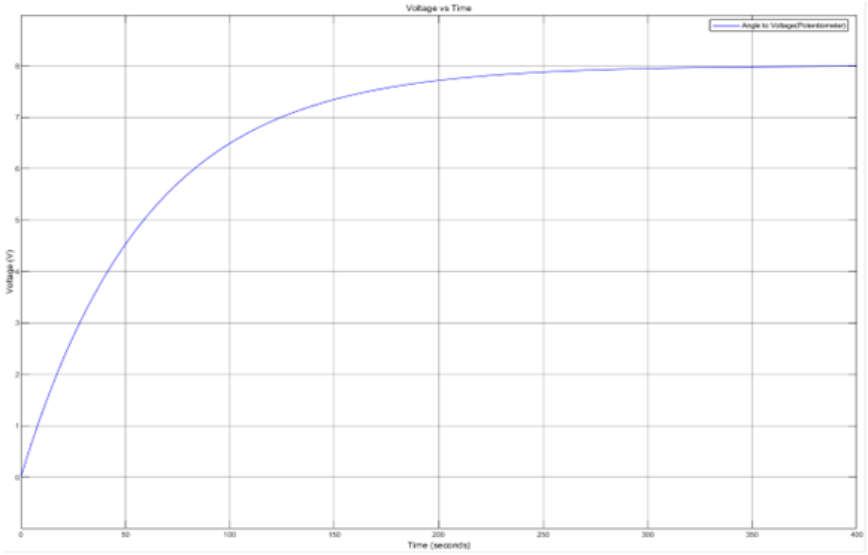

Figure 4953: PI Controller Voltage vs Time Ramp Response

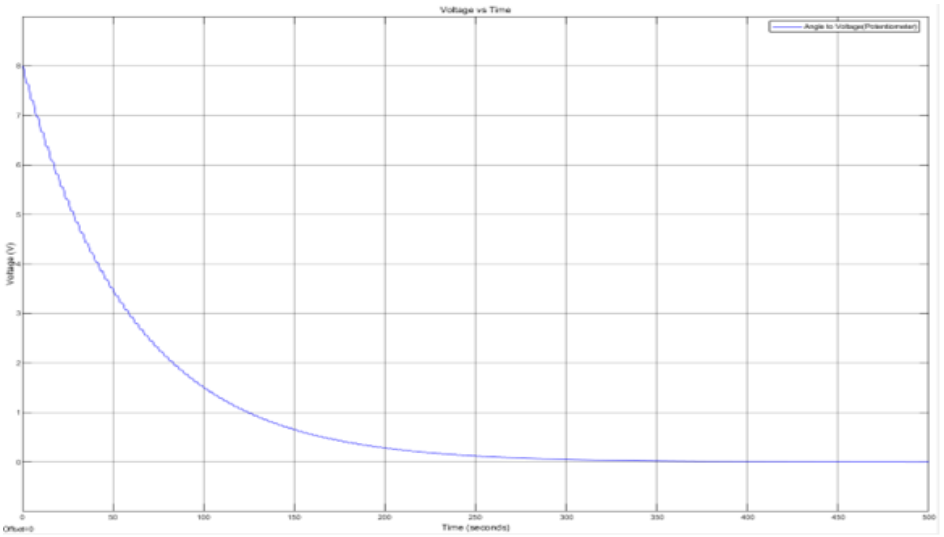

Figure 5054: PI ramp voltage response.

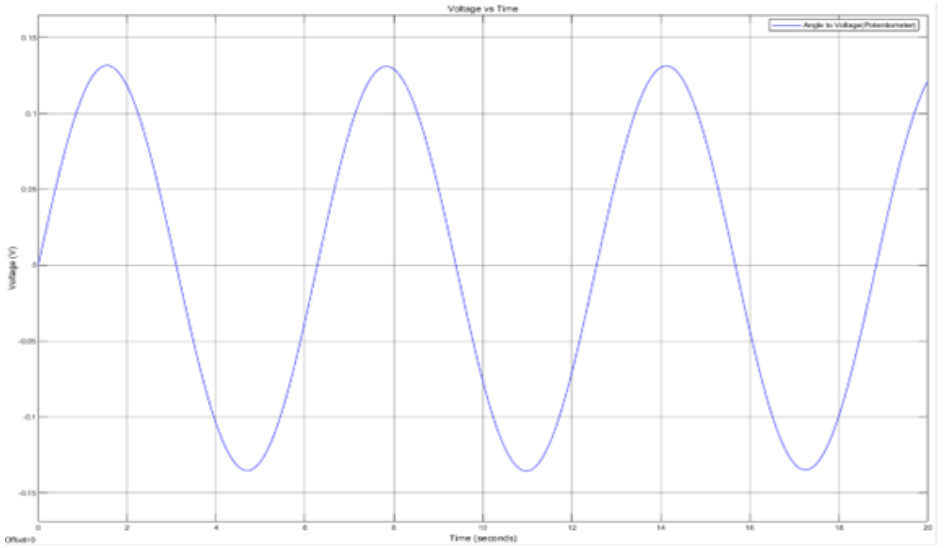

Figure 5155: PI sin voltage response.

3. PD angular and voltage response graphs

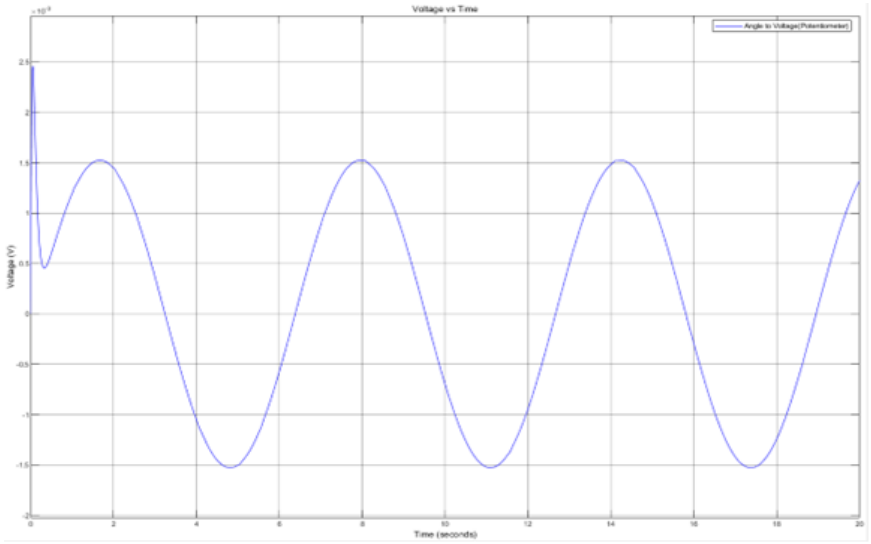

Figure 5256: PD Controller Voltage vs Time Sin Response

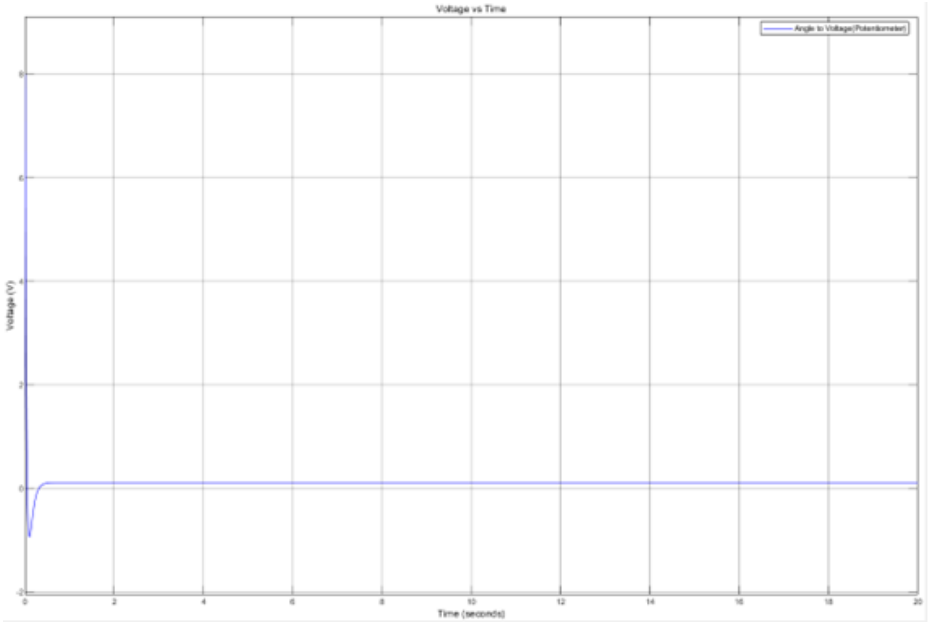

Figure 5357: PD controller Step Response.

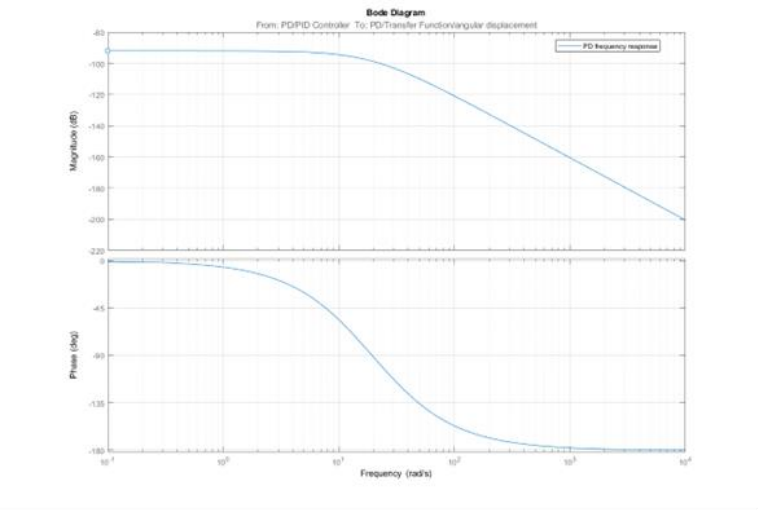

Figure 5458: PD controller closed loop frequency response.

4. PID angular and voltage response graphs

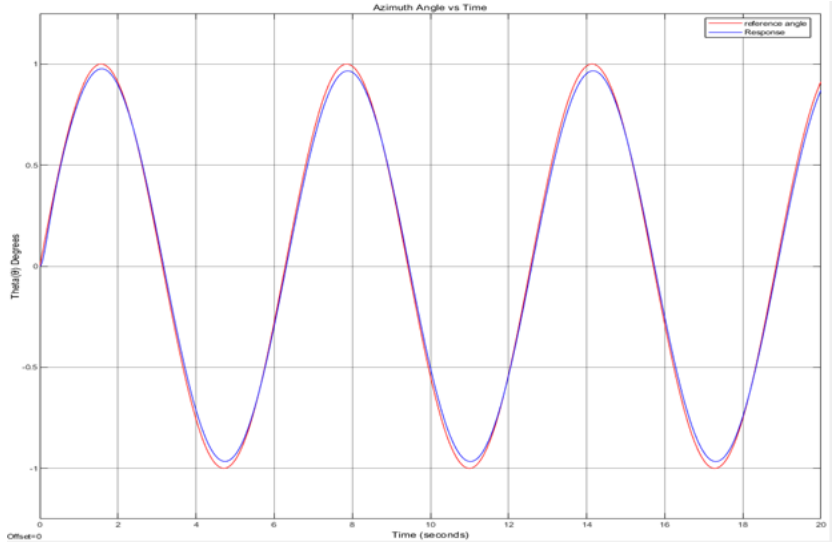

Figure 5559: PID Controller Sinusoidal Response.

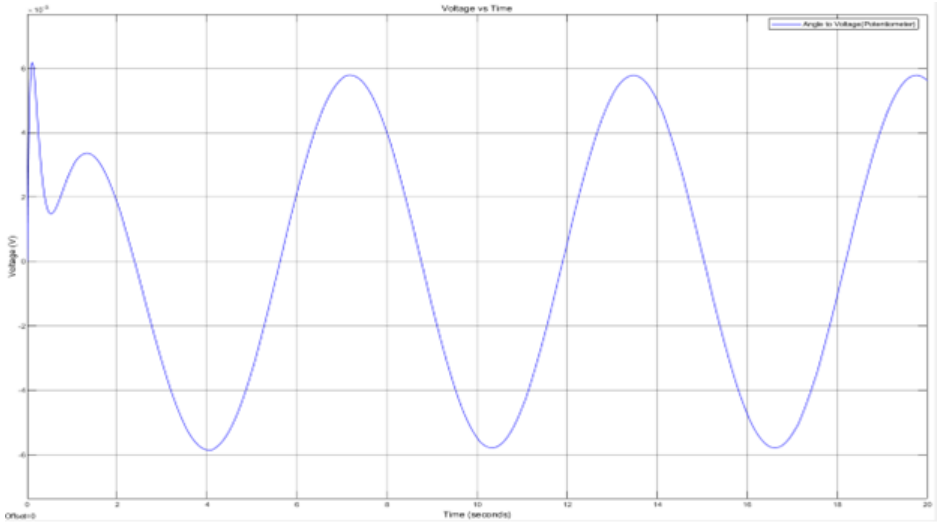

Figure 56:60 PID Controller Voltage vs Time Sin Response

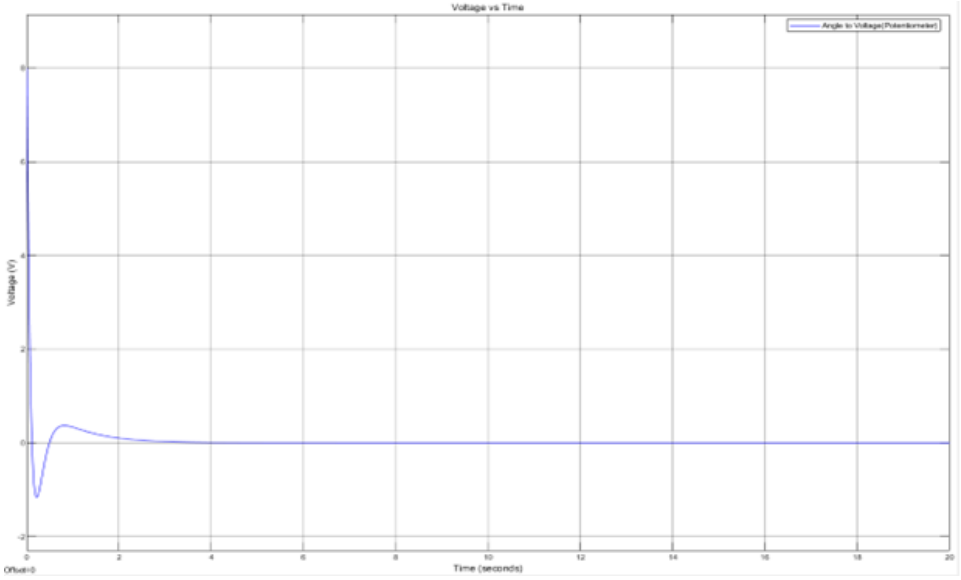

Figure 61: PID Controller Voltage vs Time Step Response

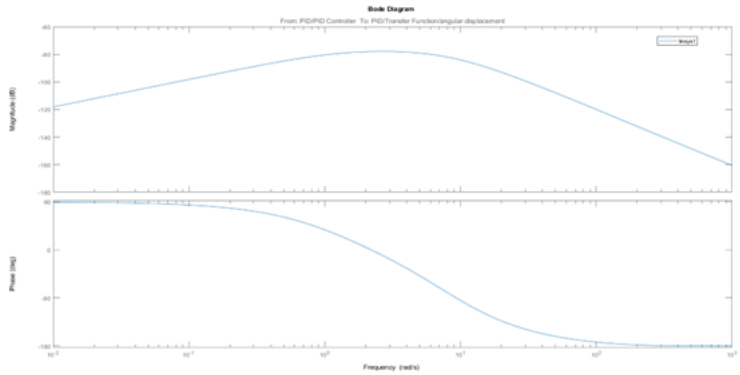

Figure 5762: PID controller Bode frequency response.

B. MATLAB CODE For Linear Open Loop System Analysis

```
% Solar panel parameters
m = 1845;            % Mass, [kg]
c = 8.1449e-6;       % Damping constant, [N*m/(rad/s)]
Jp = 399.14;         % MOI, [kg.m2]
Js = 12.45;          % MOI, [kg.m2]
g = 9.81;            % Gravitational acceleration
l = 0.05.
r = 0.07;            % Mounting Distance = l + r, [m]


% Motor parameters
Km = 0.062;          % Back EMF constant, [V/(rad/s)]
Kt = 0.062;          % Torque constant, [N*m/A]
R = 1;               % Resistance, [Ohm]
n = 62;              % Gear ratio

% Transfer Function
s = tf('s');


TF = ((n*Kt)/R)/(((Js+Jp)*s^2 + ((((n^2)*Kt*Km)/R)+c)*s+(l+r)*m*g))


den = TF.Denominator{1};

%Pole-Zero Plot
pzplot(TF)
grid

%Nyquist Plot
nyquistplot(TF)
grid

%Farzad Sagharchi (2024). Routh-Hurwitz stability criterion
(https://www.mathworks.com/matlabcentral/fileexchange/17483-routh-hurwitz-stability-criterion),
MATLAB Central File Exchange. Retrieved May 9, 2024.
%Routh Hurwitz Criterion
%% Routh-Hurwitz stability criterion
%
%  The Routh-Hurwitz stability criterion is a necessary (and frequently
%  sufficient) method to establish the stability of a single-input,
%  single-output(SISO), linear time invariant (LTI) control system.
%  More generally, given a polynomial, some calculations using only the
%  coefficients of that polynomial can lead us to the conclusion that it
%  is not stable.
%  Instructions
%  ------------
%
%  in this program you must give your system coefficients and the
%  Routh-Hurwitz table would be shown
%
%   Farzad Sagharchi ,Iran
```

```
%   2007/11/12
%% Initialization
% Taking coefficients vector and organizing the first two rows
coeffVector = den;
ceoffLength = length(coeffVector);
rhTableColumn = round(ceoffLength/2);
%  Initialize Routh-Hurwitz table with empty zero array
rhTable = zeros(ceoffLength,rhTableColumn);
%  Compute first row of the table
rhTable(1,:) = coeffVector(1,1:2:ceoffLength);
%  Check if length of coefficients vector is even or odd
if (rem(ceoffLength,2) ~= 0)
   % if odd, second row of table will be
   rhTable(2,1:rhTableColumn - 1) = coeffVector(1,2:2:ceoffLength);
else
   % if even, second row of table will be
   rhTable(2,:) = coeffVector(1,2:2:ceoffLength);
end
%% Calculate Routh-Hurwitz table's rows
%  Set epss as a small value
epss = 0.01;
%  Calculate other elements of the table
for i = 3:ceoffLength

   %  special case: row of all zeros
   if rhTable(i-1,:) == 0
      order = (ceoffLength - i);
      cnt1 = 0;
      cnt2 = 1;
      for j = 1:rhTableColumn - 1
         rhTable(i-1,j) = (order - cnt1) * rhTable(i-2,cnt2);
         cnt2 = cnt2 + 1;
         cnt1 = cnt1 + 2;
      end
   end

   for j = 1:rhTableColumn - 1
      %  first element of upper row
      firstElemUpperRow = rhTable(i-1,1);

      %  compute each element of the table
      rhTable(i,j) = ((rhTable(i-1,1) * rhTable(i-2,j+1)) - ....
         (rhTable(i-2,1) * rhTable(i-1,j+1))) / firstElemUpperRow;
   end


   %  special case: zero in the first column
   if rhTable(i,1) == 0
      rhTable(i,1) = epss;
   end
end
```

```
%%  Compute number of right hand side poles(unstable poles)
%   Initialize unstable poles with zero
unstablePoles = 0;
%   Check change in signs
for i = 1:ceoffLength - 1
   if sign(rhTable(i,1)) * sign(rhTable(i+1,1)) == -1
      unstablePoles = unstablePoles + 1;
   end
end
%   Print calculated data on screen
fprintf('\n Routh-Hurwitz Table:\n')
rhTable
%   Print the stability result on screen
if unstablePoles == 0
   fprintf('~~~~~> it is a stable system! <~~~~~\n')
else
   fprintf('~~~~~> it is an unstable system! <~~~~~\n')
end
fprintf('\n Number of right hand side poles =%2.0f\n',unstablePoles)
reply = input('Do you want roots of system be shown? Y/N ', 's');
if reply == 'y' || reply == 'Y'
   sysRoots = roots(coeffVector);
   fprintf('\n Given polynomial coefficients roots :\n')
   sysRoots
end
```

```
% Step Response
opts = stepDataOptions('StepAmplitude',-24);
step(TF,350,opts);
title('Linear Step Response')
SR_info = stepinfo(TF)
```

```
% Ramp Response
t=0:0.1:350;
alpha=1;
ramp=alpha*t;
[y,t]=lsim(TF,ramp,t);
plot(t,y)
title('Linear Ramp Response')
xlabel('time(seconds)')
ylabel('Amplitude')
grid
```

```
% Sine Response
t=0:0.1:350;
sine = -24*sin(t)
[y,t]=lsim(TF,sine,t);
```

```
plot(t,y)
title('Linear Sine Response')
xlabel('time(seconds)')
ylabel('Amplitude')
grid

% Bode plot
bode(TF)
grid

%root locus
rlocus(TF)
zeta = 0.46;
wn = 2.17;
sgrid(zeta,wn)


[k,poles] = rlocfind(TF)
sys_cl = feedback(k*TF,1)
step(sys_cl)
stepinfo(sys_cl)
```

C. Simulink Block Diagrams

1. Linear System Block Diagram

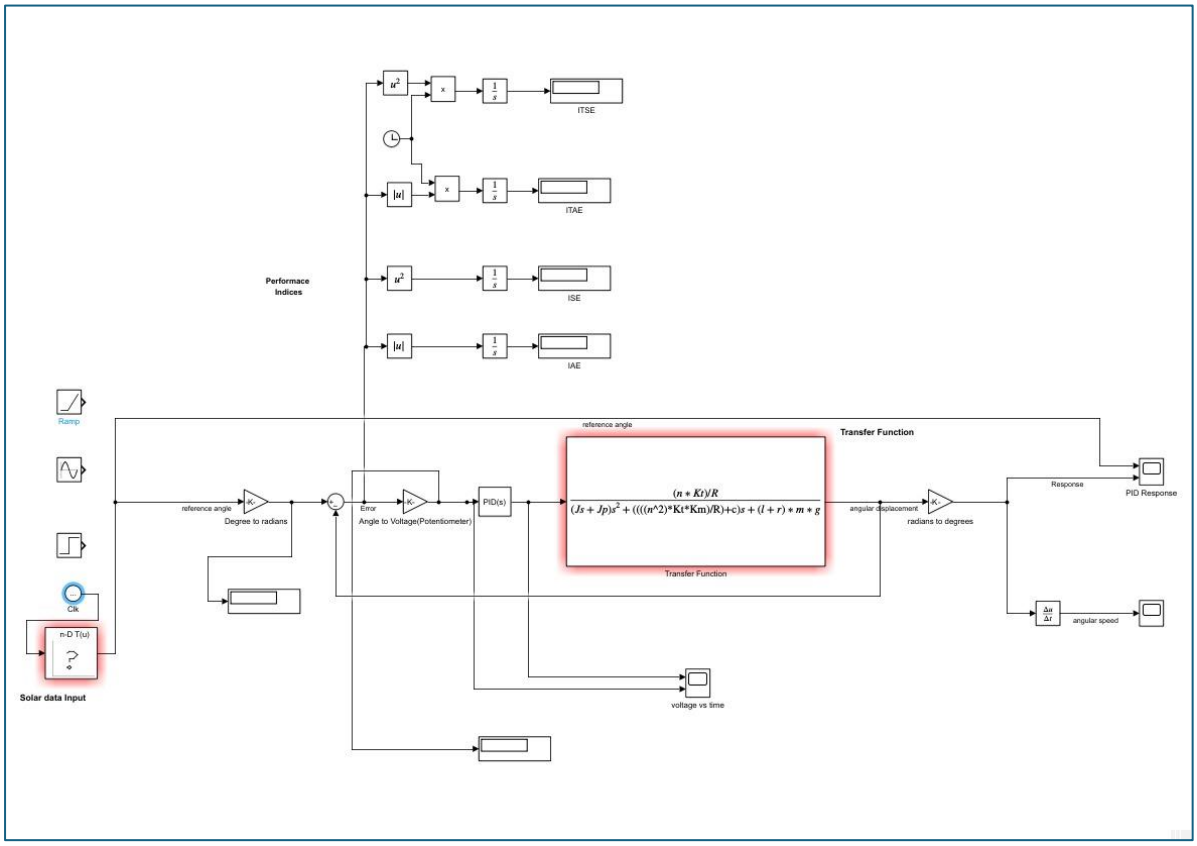

Figure 5863: PID controller Simulink diagram

2. Non-Linear System Block Diagram